BIOCHEMISTRY

The ERAD system is restricted by elevated ceramides

Jiwon Hwang[1], Brian G. Peterson[1], Jeffrey Knupp[2], Ryan D. Baldridge[1,2]*

Misfolded proteins in the endoplasmic reticulum (ER) are removed through a process known as ER-associated degradation (ERAD). ERAD occurs through an integral membrane protein quality control system that recognizes substrates, retrotranslocates the substrates across the membrane, and ubiquitinates and extracts the substrates from the membrane for degradation at the cytosolic proteasome. While ERAD systems are known to regulate lipid biosynthetic enzymes, the regulation of ERAD systems by the lipid composition of cellular membranes remains unexplored. Here, we report that the ER membrane composition influences ERAD function by incapacitating substrate extraction. Unbiased lipidomic profiling revealed that elevation of specific very-long-chain ceramides leads to a marked increase in the level of ubiquitinated substrates in the ER membrane and concomitantly reduces extracted substrates in the cytoplasm. This work reveals a previously unrecognized mechanism in which ER membrane lipid remodeling changes the activity of ERAD.

INTRODUCTION

The endoplasmic reticulum (ER) is the entry point for proteins into the secretory pathway and contains quality control systems responsible for maintaining ER homeostasis in response to stress caused by lipotoxicity and misfolded protein (*1*–*4*). Protein and lipid homeostasis are connected through the unfolded protein response (UPR) and ER-associated degradation (ERAD). ERAD directly controls lipid homeostasis through the regulated degradation of lipid biosynthetic enzymes in the sterol synthesis pathway (*5*–*7*). This includes the HMG CoA-reductase (HMGCR) isozyme (Hmg2 in yeast) and squalene monooxygenase (Erg1 in yeast), which undergo degradation by ERAD in response to multiple metabolites of the sterol synthesis pathway. In yeast, additional ergosterol biosynthetic enzymes are regulated by ERAD systems (Erg1, Erg3, Erg5, Erg11, and Erg25) to control metabolic flux, and many of these ERAD-centered regulatory pathways are conserved for cholesterol regulation in mammals (*5*, *8*–*11*). In addition to regulating lipid biosynthetic enzymes, ERAD continuously monitors nascent protein folding in the secretory pathway and targets terminally misfolded and unassembled proteins for clearance before they induce toxicity (*2*). When misfolded and unwanted proteins accumulate in the ER and exceed the capacity of ERAD, protein folding stress will eventually activate the UPR (*12*).

The essential features of ERAD are highly conserved among eukaryotes. Work in *Saccharomyces cerevisiae* demonstrated that substrates are recognized and degraded through different pathways, depending on whether their misfolded domain is luminal (ERAD-L), transmembrane (ERAD-M), cytosolic (ERAD-C), or spatially restricted to the inner nuclear membrane (ERAD-INM). These pathways use different ubiquitin ligases: ERAD-L and ERAD-M use the Hrd1 ligase; ERAD-C uses the Doa10 ligase, and ERAD-INM uses the Asi ligase complex (*9*, *13*–*17*). These ubiquitin ligases are multispanning integral membrane proteins with a RING finger domain located in the cytoplasm. All ERAD pathways converge once the substrates are on the cytosolic face of the ER, where they require ubiquitination machinery, the AAA-ATPase(Adenosine triphosphatase Associated with diverse cellular Activities) Cdc48, Cdc48 cofactors, and the proteasome for degradation (*18*–*21*).

Among the ERAD systems, Hrd1-centric processes are best understood through decades of work using genetic, biochemical, proteomic, and structural analyses (*13*, *22*–*27*). ERAD-L substrates are degraded by Hrd1 in complex with three other membrane proteins, Hrd3, Usa1, and Der1. Hrd1 is a ubiquitin ligase and the central component of the ERAD-L and ERAD-M systems. Hrd1 forms a retrotranslocation channel (retrotranslocon) consisting of a hetero-oligomer (with Der1) or homo-oligomer that is controlled by cycles of autoubiquitination, deubiquitination, and substrate binding (*23*, *26*, *28*–*31*). ERAD-L substrates are recruited to the Hrd1 complex by Hrd3, a single-spanning membrane protein containing a large luminal domain that interacts with substrates and Hrd1 (*32*). In addition, Hrd3 functions outside substrate recruitment by mitigating Hrd1 autoubiquitination activity (*22*). Deubiquitination of Hrd1 by Ubp1 appears to be controlled by Usa1, another integral membrane protein in the Hrd1 complex (*28*). Usa1 also facilitates hetero-oligomerization of the Hrd1 retrotranslocon by serving as a linker between Hrd1 and the rhomboid pseudoprotease Der1 (*23*, *33*, *34*). ERAD-M substrates are proposed to enter the Hrd1 channel laterally from the lipid phase, and by definition, polypeptides of ERAD-M substrates are already exposed in the cytosol. In contrast to ERAD-L, ERAD-M substrates do not seem to strictly require either Der1 or Hrd1 retrotranslocation function. Instead, another rhomboid pseudoprotease, Dfm1, appears to facilitate the dislocation/extraction of ERAD-M substrates (*35*, *36*).

The energetics of ERAD-mediated retrotranslocation and extraction from the ER membrane likely depend on the membrane composition. Membrane protein function is influenced by the lipid bilayer, through specific lipid interactions with individual proteins/complexes (*37*, *38*) and through the biophysical properties of the membrane (*39*, *40*). Eukaryotes contain exquisitely specific lipid-responsive ER sensors for controlling fluctuations in lipid levels. For example, in budding yeast, the ER-associated transcription factor Opi1 controls the flux of lipid metabolites into storage and membrane lipids by sensing cellular levels of phosphatidic acid (*41*). Two paralogous yeast transcription factors, Mga2 and Spt23, sense lipid acyl chain saturation and respond by transcriptionally

[1]Department of Biological Chemistry, University of Michigan Medical School, 1150 W Medical Center Drive, Ann Arbor, MI 48109, USA. [2]Cellular and Molecular Biology Program, University of Michigan Medical School, Ann Arbor, MI 48109, USA.
*Corresponding author. Email: ryanbald@umich.edu

regulating the production of the fatty acid desaturase Ole1 (stearoyl–CoA desaturase-1, SCD1 in mammals) (*42*). The ER membrane is a heterogeneous mixture of lipids across leaflets of the lipid bilayer and laterally within a face of the lipid bilayer. Relative to other cellular membranes, the ER is thinner, has a higher proportion of phospholipids compared to sterols and sphingolipids, and is proposed to be relatively flexible to accommodate diverse processes such as protein translocation and integration of membrane proteins (*43*). Emerging evidence suggests that lipids and membrane proteins exert control over one another. Rhomboid proteases are an archetype of this idea; rhomboids are both regulated by the composition of the lipid bilayer (*44*) and can manipulate the lipid bilayer to break the diffusion "limit" (*45*). In ERAD, the rhomboid pseudoproteases Der1 and Dfm1 are proposed to "thin" the lipid bilayer to enable protein retrotranslocation and extraction, but experimental evidence of this principle is still absent (*23*, *46*, *47*).

The composition of the ER membrane is tightly controlled, and alterations in ER protein and lipid homeostasis are closely associated with obesity, diabetes, cancer, and neurodegenerative diseases (*48–51*). Aberrant ERAD function is also associated with these diseases (*52*). Therefore, insight into the interplay between lipid composition and protein quality control could revolutionize our understanding of these common, debilitating pathologies. On the basis of the influence of lipid composition on the activity of many other integral membrane proteins (*41*, *53*, *54*), we hypothesized that the ER membrane composition could regulate the function of the ER membrane–embedded Hrd1-ERAD complex. Here, we demonstrate that changes in the composition of the ER membrane can impair the function of the Hrd1-centric ERAD system. Using pharmacological and genetic manipulation to change the composition of the ER membrane, combined with unbiased lipidomic analysis, we find that elevation of specific very-long-chain ceramides restricts ERAD function, leading to substrate accumulation. This accumulation was not due to impaired ERAD complex assembly; under increased ceramide levels, the ERAD complex remained intact, and Hrd1 ubiquitination activity persisted. Rather, ubiquitinated ERAD substrates accumulated in the ER membrane, indicating that the extraction of substrates into the cytosol for degradation was disrupted under conditions with elevated ceramide levels. Ceramide accumulation occurs under various physiological and pathophysiological conditions [e.g., heat shock, obesity, type 2 diabetes, cardiovascular disease, cancer, and Farber disease (*55–63*)]. Dysfunction of ERAD is associated with similar pathophysiological conditions including metabolic syndromes (obesity and type 2 diabetes), infectious diseases, cancer, and neurological illnesses (Alzheimer's disease and Parkinson's disease) (*52*). Thus, our work reveals an intriguing interplay between lipid homeostasis and
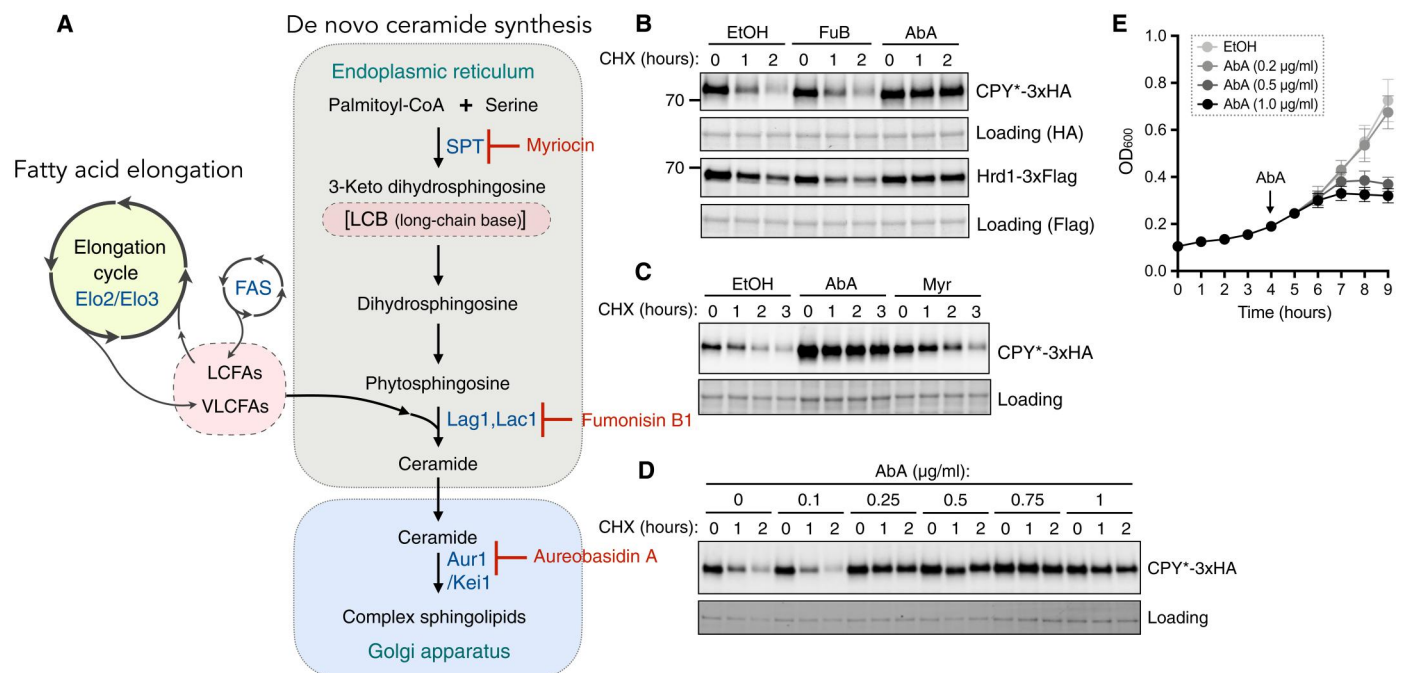
Fig. 1. IPC synthase inhibition impairs Hrd1-centric ERAD. (A) Diagram of the sphingolipid biosynthesis pathway in *S. cerevisiae*. Metabolic intermediates and complex sphingolipids are indicated in black lettering, while enzymes are in blue. The reaction cycle that produces very-long-chain fatty acids is indicated in the green circle. The target processes of three inhibitors [myriocin (Myr), fumonisin B1 (FuB), and aureobasidin A (AbA)] are shown in red. SPT, serine palmitoyltransferase complex (composed of Lcb1, Lcb2, and Tsc3); Lag1 and Lac1, ceramide synthases; Aur1/Kei1, IPC synthase complex; Elo2 and Elo3, very-long-chain fatty acid elongases; FAS, fatty acid synthase; LCFAs, long-chain fatty acids; VLCFAs, very-long-chain fatty acids. **(B)** The degradation of CPY*-3xHA and Hrd1-3xFlag was monitored following the addition of cycloheximide (CHX) at the indicated time points. Hrd1-3xFlag and CPY*-3xHA were expressed from centromeric plasmids under endogenous promoters in *hrd1Δ* cells. Cells were pretreated with ethanol (EtOH; vehicle control), FuB at 50 μM overnight, or AbA (0.5 μg/ml) for 2 hours before cycloheximide treatment. The relative loading amount of the total protein was visualized by stain-free dye. **(C)** As in (B) but cells were treated with ethanol, AbA (0.5 μg/ml), or Myr (0.5 μg/ml) for 2 hours before cycloheximide treatment. **(D)** As in (B) except that cells were pretreated with AbA at the indicated concentrations for 2 hours before cycloheximide treatment. **(E)** Growth of cells in synthetic liquid media supplemented with AbA at the indicated concentrations was followed by OD_{600} (optical density at 600 nm). Data are presented as means ± SD from three experiments. Each immunoblot is representative of at least three independent biological replicates. See also fig. S1.

protein quality control and defines a unique regulatory mechanism for ERAD activity.

RESULTS

Inactivation of the inositol phosphorylceramide synthase Aur1 leads to impaired ERAD function

The ER membrane is the primary site of lipid biosynthesis and is primarily composed of phospholipids with a correspondingly low sterol and sphingolipid content (64). The ER is also a major site of protein quality control for membrane or secretory pathway proteins. Because ERAD systems are embedded in the ER lipid bilayer, we hypothesized that under specific circumstances, lipids may control the function of this complex. There have been considerable efforts over several decades to examine the complex regulatory steps in sterol synthesis, leading to the identification of numerous lipids involved in the regulation of specific ERAD substrates (6, 65). In each case, the identified lipids influenced the folding of ERAD substrates rather than the activity of their respective ERAD systems. With the extensive literature on the sterol biosynthetic pathway lacking evidence for sterol-mediated control of ERAD activity, we shifted our attention to the other low-abundance lipids in the ER: those in the sphingolipid synthesis pathway. We disrupted the de novo sphingolipid biosynthesis pathway using the available pharmacological agents myriocin, fumonisin B1 (FuB), and aureobasidin A (AbA). Each of these agents blocks the formation of complex sphingolipids by inhibiting different steps in the pathway: myriocin by inhibiting serine palmitoyl transferase, FuB by inhibiting ceramide synthases, and AbA by inhibiting Aur1, the inositol phosphorylceramide (IPC) synthase (Fig. 1A) (66). To examine the effect of perturbing sphingolipid biosynthesis on Hrd1-centric ERAD, we analyzed the degradation of a model Hrd1 substrate, carboxypeptidase Y* (CPY*), using a cycloheximide chase in cells treated with these pharmacological agents (67). In untreated cells, the half-lives of CPY* and Hrd1 were ~30 and ~90 min, respectively, consistent with previous reports (Fig. 1B) (22, 68). Treatment with FuB did not impair the degradation of CPY* or Hrd1 (Fig. 1B). Similarly, treatment with myriocin did not prevent the degradation of CPY* (Fig. 1C), although myriocin was able to inhibit cell growth (fig. S1). In contrast, the addition of AbA prevented the degradation of both CPY* and Hrd1 itself (Fig. 1, B and C). These findings provide the first evidence that specific sphingolipid biosynthetic precursors (possibly ceramides), rather than reduction in the levels of complex sphingolipids as a whole, can influence and inhibit ERAD activity.

Stabilization of CPY* was observed following a 2-hour pretreatment with AbA concentrations at or above 0.25 μg/ml (Fig. 1D). AbA concentrations above 0.25 μg/ml stabilize CPY* consistently; however, treatments at or above 0.5 μg/ml caused cellular growth defects if cells were treated beyond 3 hours (Fig. 1E), probably from a combination of increased ceramides and reduced complex sphingolipids (69). Therefore, future cycloheximide chase experiments were conducted with a 2-hour pretreatment of cells with AbA (0.5 μg/ml). To examine the effect of AbA on each ERAD pathway, we followed the degradation of a panel of ERAD substrates for ERAD-L (CPY*; Fig. 1B), ERAD-M (Erg3; Fig. 2A), ERAD-INM (Erg11; Fig. 2B), and ERAD-C pathways (Erg1 and Ste6*; Fig. 2, C and D). Cycloheximide chase experiments showed that AbA treatment stabilized substrates in the ERAD-L, ERAD-M, and ERAD-

INM pathways. In the ERAD-C pathway, Erg1 was stabilized by AbA treatment, while the ERAD-C substrate Ste6* was still degraded. To test whether the ubiquitin proteasome system remained functional with AbA treatment, we followed the degradation of a cytosolic ubiquitin-dependent proteasomal substrate called Cit2 (Fig. 2E) (70) and an engineered cytosolic ubiquitin-independent proteasomal substrate called UBL-mScarlet-Su9 (Fig. 2F) (71). These results demonstrate that AbA treatment does not impair the ubiquitin proteasome system, given that ubiquitin-dependent and ubiquitin-independent degradation by the proteasome remains functional. To exclude potential off-target effects of AbA, we used a previously characterized AbA-resistant Aur1 mutant (Aur1^R) (72, 73). In wild-type cells, we expressed a second copy of either wild-type Aur1 or Aur1^R. Cells expressing Aur1^R were resistant to AbA-related growth defects observed in Aur1^{WT} cells treated with AbA, confirming the AbA-resistant phenotype of this mutant (Fig. 2G). With AbA treatment in the presence of the Aur1^R variant, CPY* and Erg3 were degraded as in untreated or wild-type cells, providing strong evidence that the ERAD inhibition caused by AbA was directly linked to Aur1 inhibition rather than to other off-target effects (Fig. 2H). Together, these data demonstrate that Aur1 inhibition by AbA treatment stabilizes ERAD substrates by specifically impairing ERAD systems and not the ubiquitin proteasome system.

The UPR is mildly activated when the IPC synthase complex is disabled

The UPR sensor Ire1 directly responds to ER stress to restore proteostasis and to rebalance the ER membrane composition (74). To test whether AbA-dependent ERAD inhibition was caused by failure to activate the UPR, we constructed a modified fluorescent UPR reporter using the fluorescent protein GFPfast controlled by a 4x repeat of the UPR element (4xUPRE) upstream of the *CYC1* promoter [UPRE-GFP (green fluorescent protein)] (75). We can monitor the induction of this reporter via flow cytometry. The UPRE-GFP reporter accurately responded to known UPR-inducing conditions including genetic (*hrd1Δ*), misfolded ER protein (CPY*), and chemical [dithiothreitol (DTT)] ER stressors (fig. S2, A and B). Consistent with previous reports, DTT treatment resulted in maximum activation of UPRE-GFP. We next followed the induction of the UPRE-GFP in cells treated with AbA over 3 hours. AbA treatment induced UPRE-GFP after a minimum of 2 hours with AbA (Fig. 2I), with a UPR induction intensity comparable to that of a *hrd1Δ* strain (Fig. 2J). Moreover, the UPR was still active in cells treated with both AbA and DTT, demonstrating that AbA treatment did not prevent the induction of the UPR (Fig. 2K). AbA treatment led to additional UPR induction in cells expressing catalytically inactive Hrd1 (C399S) (fig. S2, C and D). We interpret this result to mean that disruption of lipid homeostasis by Aur1 inactivation activates the UPR, independently of protein accumulation caused by nonfunctional ERAD. Together, these findings support not only the idea that inactivation of Aur1 induced mild ER stress but also the idea that ERAD substrate stabilization did not result from incapacitated UPR.

Genetic disruption of the IPC synthase complex inhibits ERAD

Sphingolipids are essential components of cellular membranes, and disrupting the biosynthesis (as with AbA treatment) will eventually
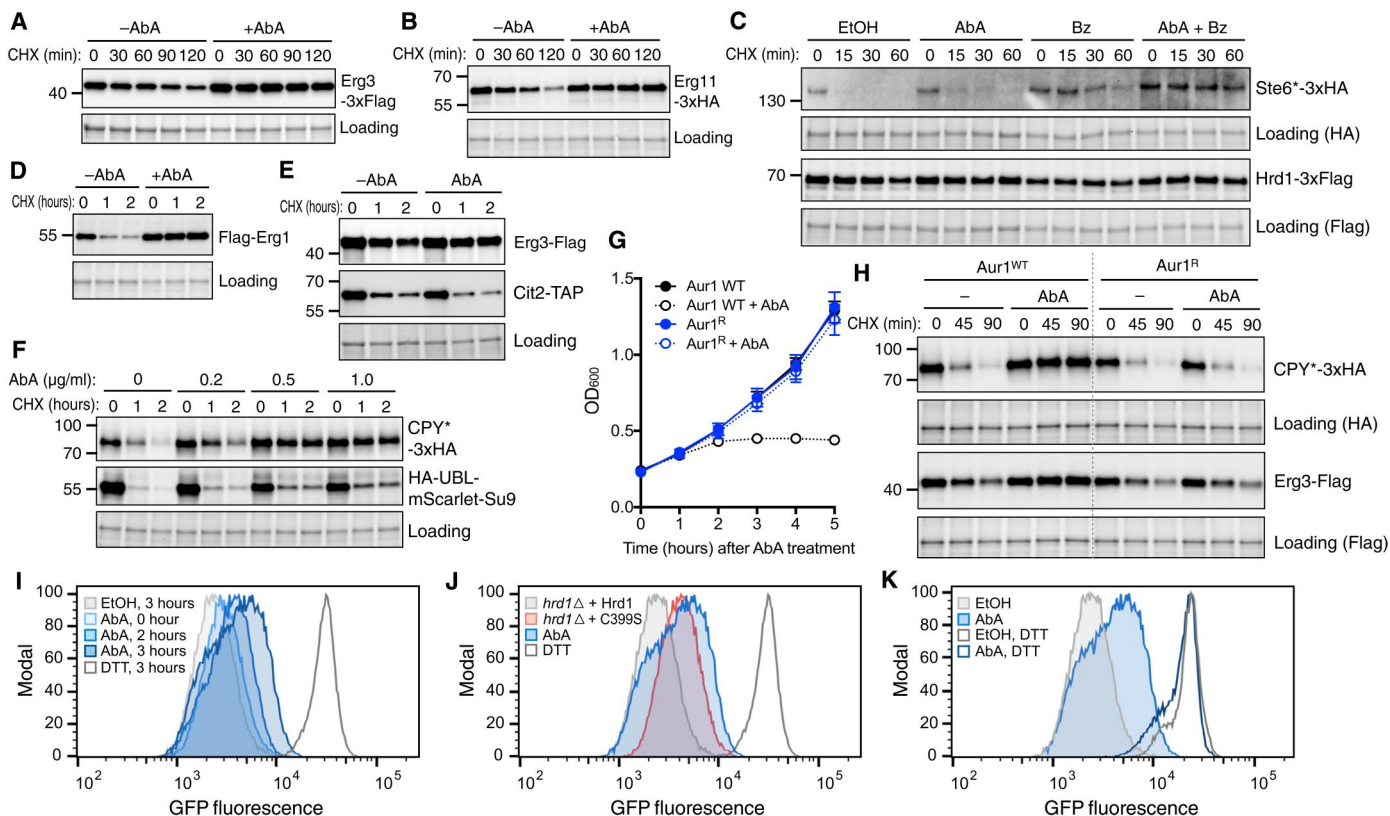
Fig. 2. Pharmacological inhibition of Aur1 disrupts multiple ERAD pathways. (**A**) The degradation of Erg3-3xFlag was monitored after the addition of cycloheximide. Erg3-3xFlag was expressed from the endogenous promoter on a centromeric plasmid in wild-type (WT) cells. Total protein was visualized by stain-free dye. (**B**) As in (A) but with Erg11-3xHA. (**C**) Ste6*-3xHA from an ADH1 promoter and Hrd1-3xFlag under its endogenous promoter were expressed from centromeric plasmids in *hrd1Δpdr5Δ* cells. Cells were pretreated for 2 hours with ethanol or AbA and, where indicated, were pretreated with 50 μM bortezomib (Bz) for 30 min before cycloheximide treatment. (**D**) As in (A) but with Flag-Erg1. (**E**) As in (A) but with Erg3-3xFlag and Cit2-TAP. Erg3-3xFlag was expressed on a centromeric plasmid in a Cit2-TAP strain. (**F**) As in (A) but with CPY*-3xHA and HA-UBL-mScarlet-Su9. (**G**) Growth curve of Aur1^WT or Aur1^R cells in liquid media. AbA was used at 0.5 μg/ml. Data are presented as means ± SD from three experiments. (**H**) Aur1^WT or Aur1^R was integrated into a wild-type strain. Degradation of CPY*-3xHA and Erg3-3xFlag was followed as in (A). (**I**) Hrd1-3xFlag was integrated into *hrd1Δ* cells expressing a UPR reporter (4xUPRE-GFPfast); treated with ethanol, AbA (1 μg/ml), or 2 mM dithiothreitol (DTT) for the indicated time periods; and analyzed by flow cytometry. (**J**) Hrd1-3xFlag or catalytically inactive Hrd1 (C399S) was integrated into a *hrd1Δ* strain with an integrated UPR reporter. Cells were treated with ethanol, AbA, or DTT for 3 hours. (**K**) The Hrd1-3xFlag–integrated *hrd1Δ* cells expressing the UPR-reporter were treated for 3 hours with ethanol, AbA, or a combination of ethanol or AbA with DTT following 1 hour of pretreatment. Each is representative of at least three independent biological replicates. See also fig. S2.

lead to cell death (*69*). To test whether AbA-dependent ERAD inhibition is a secondary effect from cell death, we used a genetic mutation of Aur1 function. Together, the IPC synthase complex is formed by Aur1 and its cofactor Kei1 (*76*). We generated a previously characterized Kei1 temperature-sensitive allele (*kei1-1*) that impairs Aur1 function at elevated temperatures (*76*). In our strains, the *kei1-1* allele was hypomorphic and displayed slow growth relative to the wild type at both permissive (26.5°C) and nonpermissive (32°C) temperatures with a more severe growth defect observed at 32°C (Fig. 3A). Degradations of Hrd1, CPY*, and Erg3 were all impaired in *kei1-1* at both temperatures (Fig. 3, B to G). Degradation of the cytosolic proteasomal substrate UBL-mScarlet-Su9 was similar to that of wild-type cells in *kei1-1*, demonstrating that the proteasome remained active at both permissive and restrictive temperatures (Fig. 3, H and I). Together, these data indicate that both genetic and pharmacologic Aur1 inactivation prevented substrate degradation by specific ERAD pathways. Aur1 inactivation causes ceramide accumulation and disrupts complex

sphingolipid biosynthesis but does not cause a global defect in the ubiquitin proteasome system.

Elevation of very-long-chain ceramide is negatively associated with ERAD activity

To identify candidate lipid species that could affect ERAD function, we carried out untargeted shotgun lipidomic profiling of lipid metabolites by absolute quantification of individual molecular lipid species. Our analysis encompassed a wide array of lipid classes, including sphingolipids, ceramides, neutral lipids, phospholipids, lysophospholipids, and sterols (20 classes and 618 subspecies). First, we confirmed the effect of AbA by analyzing the degradation of both Hrd1 and its substrates by immunoblotting before lipid extractions (fig. S3, A and B). Next, we confirmed previously reported results that treatment with AbA reduced the complex sphingolipids in our experiments (fig. S3, C and D). Because AbA is reported to target Aur1, we examined the two substrate classes for Aur1, ceramides and phosphatidylinositols. In the untreated strains, the
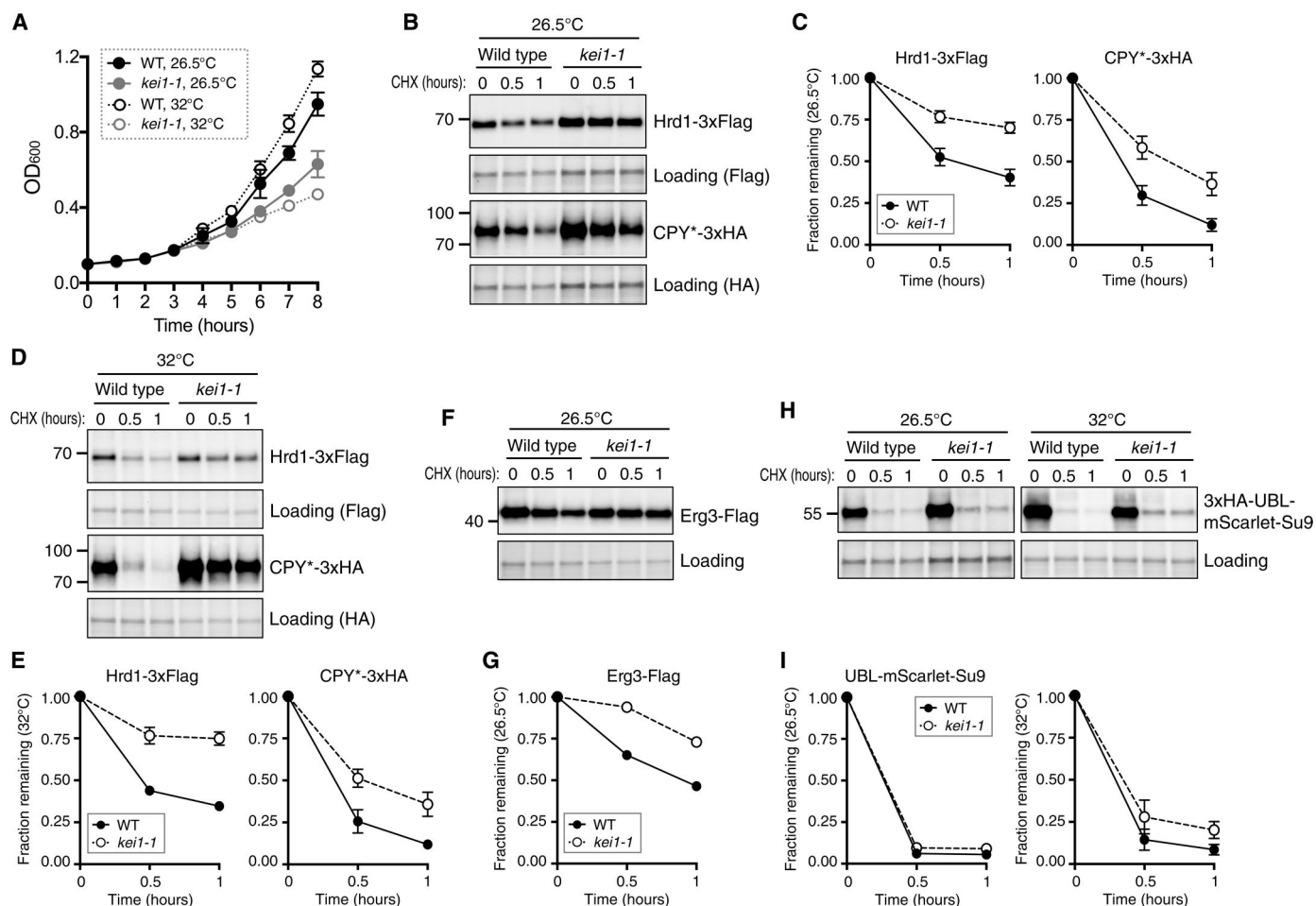
Fig. 3. Genetic disruption of *KEI1*, an essential component of IPC synthase, impairs ERAD. (**A**) Growth was measured by OD_{600} for wild-type and *kei1-1* cells in liquid media. For growth assays at restrictive temperature (32°C), cells were cultured at permissive temperature (26.5°C) for the first 3 hours and then shifted to 32°C. Data are presented as means ± SD from three experiments. (**B**) Hrd1-3xFlag and CPY*-3xHA were expressed from centromeric plasmids in either wild-type or *kei1-1* cells. Cells were grown at the permissive temperature (26.5°C) before cycloheximide treatment. (**C**) Quantification of (B). (**D**) As in (B) but following the degradation at the restrictive temperature (32°C). (**E**) Quantification of (D). (**F**) As in (B) but following the degradation of Erg3-3xFlag. (**G**) Quantification of (F). (**H**) As in (B) but following the degradation of HA-UBL-mScarlet-Su9 at the indicated temperatures. (**I**) Quantification of (H). Each immunoblot is representative of at least three independent biological replicates. For each quantification, data from at least three experiments are presented as means ± SEM.

most common ceramides were Cer 42:0;2 (42, number of carbons in fatty acid chain; 0, number of acyl chain carbon-carbon double bonds; and 2, number of hydroxy groups) and Cer 44:0;4. Together, these lipids accounted for around 60% of the total ceramides (fig. S3E) and were increased approximately two-fold with AbA treatment (fig. S3F). The most common phosphatidylinositols (PI32:1;0 and PI34:1;0) accounted for around 50% of the cellular phosphatidylinositol and were increased 1.3- and 1.7-fold, respectively, during AbA treatment (fig. S3, C and D, and dataset S1). Next, we grouped the 618 lipids quantified into broad classes and plotted their relative change compared to the untreated control (Fig. 4A). We found that, in most classes, at least a few specific lipids were either increased or decreased by two-fold or more (Fig. 4A and fig. S3, C and D).

To narrow down our candidates to either lipid classes or individual lipids, we reasoned that both FuB and AbA would have similar effects on broader lipid profiles, with the largest differences being in the early stages of the sphingolipid synthesis. On the basis of our

previous FuB treatment and positioning within the sphingolipid synthesis pathway (Fig. 1, A and B), we hypothesized that cotreatment of FuB with AbA would prevent the inactivation of ERAD. Unexpectedly, we found that cotreatment of cells with both FuB and AbA still prevented the degradation of our model ERAD substrate (fig. S3B). Again, we performed lipidomic profiling on cells treated with only FuB or with both FuB and AbA together. By comparing both the broad classes and specific lipid species increased in treatment with AbA only, we found that there were only a few lipid species increased, or decreased, two-fold in common between the treatments (Fig. 4B and fig. S3D). These lipids belonged within the diacylglycerols, phosphatidic acids, phosphatidylinositols, ceramides, and IPCs.

Somewhat unexpectedly, treatment with FuB also resulted in elevated ceramides (Fig. 4, B and C), although FuB is reported to inhibit ceramide biosynthesis in yeast (Fig. 4B and fig. S3, C and D). While examining ceramide species individually, we recognized that FuB treatment elevated shorter-chain ceramide species but not

Fig. 4. Lipidomic profiling reveals that very-long-chain ceramides can control ERAD. (**A** and **B**) Comparative lipidomics of wild-type cells treated with ethanol or AbA (0.5 μg/ml) for 2 hours. Mean values of the 618 lipid subspecies that are shown as fold change relative to the control are shown as dots. Lipids with greater than a two-fold change are shown in color, while those with less than a two-fold change are shown in gray. Lipid subspecies were grouped on the basis of lipid class. Fold change values are calculated from the mean of two independent biological replicates. Bright red dots indicate ceramides C42:0;2 and C44:0;4. (**B**) As in (A) but instead with 50 μM FuB for 16 hours before ethanol or AbA treatment for 2 hours. The combination treatment was normalized to the FuB-only treatment. (**C**) Sixteen subspecies of ceramides were grouped on the basis of carbon chain length. Mean values are shown as mole percent values. (**D**) As in (A) but with wild-type cells containing an integrated Aur1WT-3xFlag or an AbA-resistant variant (Aur1R-3xFlag). Bright red dots indicate C42:0;2 and C44:0;4 from an ERAD-defective group (Aur1WT treated with AbA). Blue- or green-circled gray dots indicate C42:0;2 and C44:0;4 from ERAD-functional strains (Aur1R treated with ethanol or AbA). (**E**) As in (C) but with Aur1WT and Aur1R cells. (**F**) As in (A) but wild-type and *kei1-1* cells at low and high temperatures. (**G**) As in (C) but with wild-type and *kei1-1* cells. (**H**) Relative change in levels of C42:0;2 and C44:0;4 in each lipidomic dataset is illustrated. w indicates wild-type *KEI1* and ts indicates temperature-sensitive *kei1-1*. (**I**) Untargeted lipidomic analysis revealed global changes in lipid class, illustrated as a heatmap. LC, long-chain; VLC, very-long-chain. See also figs. S3 to S5.

very-long-chain ceramides (≥C42). This is consistent with previous studies that demonstrated that FuB treatment drives the accumulation of abnormal, shorter-chain ceramides (77) and of very-long-chain fatty acids and sphingosine bases (78). Comparing the FuB and FuB + AbA treatment conditions, we were able to eliminate many specific lipid species as candidate lipids, but Cer 42:0;2 and Cer 44:0;4 were still elevated even with cotreatment. The FuB treatment condition allowed us to exclude very-long-chain fatty acids and sphingosine bases as the cause for ERAD inhibition, although they were not present in our lipidomic analysis.

Next, we analyzed wild-type cells transformed with Aur1^{WT}-3xFlag or an AbA-resistant variant (Aur1^R-3xFlag) and each strain either untreated or treated with AbA. We confirmed the effect of AbA by analyzing the degradation of CPY* (fig. S3G) and verifying that levels of the complex sphingolipids IPC and MIPC (mannosyl-inositolphosphorylceramide) were reduced in AbA-treated cells but not in the Aur1^R variant (fig. S3, H and I). As previously reported, levels of M(IP)$_2$C [mannosyl-di-(inositol-phosphoryl)ceramide] were similar with AbA treatment (79). We found that ceramide levels in cells expressing Aur1^{WT}-3xFlag were reduced relative to those in true wild-type cells, likely because the second copy of Aur1 (endogenous Aur1 and Aur1^{WT}-3xFlag) increases the flux in the pathway (compare fig. S3E to fig. S3J). AbA treatment markedly increased both Cer 42:0;2 and Cer 44:0;4 species in the control cells but not in the Aur1^R cells (Fig. 4, D and E, and fig. S3K). After we analyzed the lipid profiles for this grouping, very-long-chain ceramide, cytidine diphosphate diacylglycerol, and lysophosphatidylinositol remained as candidates.

We used the *kei1-1* allele for genetic disruption of the same biosynthetic step as AbA treatment (see Figs. 1 and 3) for untargeted lipidomic profiling at low (26.5°C) and high (32°C) temperatures. We confirmed that the *kei1-1* allele disrupted ERAD by analyzing the degradation of Hrd1 using immunoblotting before lipid extraction (fig. S4A). Then, we confirmed that *kei1-1* reduced the complex sphingolipids (fig. S4, B and C). When we focused on the specific lipids consistently identified in the previous lipidomic datasets, we found that ceramides were the only class of lipids consistently associated with inhibition of ERAD (Fig. 4F and fig. S4, B and C). We examined the predominant ceramide species for each temperature-matched pair of samples; both Cer 42:0;2 and Cer 44:0;4 were increased in *kei1-1* cells at 32°C and, to a lesser extent, at 26.5°C (Fig. 4, F and G, and fig. S4D). Following the lipidomic profiling experiments, the only lipid species with increases or decreases that were clearly correlated with ERAD inhibition were very-long-chain ceramides (Fig. 4H).

Very-long-chain ceramides were the primary candidates for lipids inhibiting ERAD activity, and each contained saturated acyl chains. Saturated lipids or the ratio between unsaturated and saturated fatty acids in the membrane can influence the biophysical properties of the membrane and induce ER stress (7, 53, 54). From our lipidomic experiments, we asked whether the degree of acyl chain saturation was likely to influence ERAD activity and found no association between the level of acyl chain saturation and ERAD function (fig. S5, A to C).

Together, these experiments illuminated the consistent, important, and specific role for very-long-chain ceramides across each of our lipidomic datasets, primarily Cer 42:0;2 and Cer 44:0;4 (Fig. 4H). Lipidomic changes were summarized as a heatmap

reflecting their respective log fold change (Fig. 4I; raw data available in dataset S1).

Accumulation of very-long-chain ceramide restricts ERAD function

On the basis of the lipidomic experiments, very-long-chain ceramides (Cer 42:0;2 and Cer 44:0;4) were the primary candidates, but our lipidomic analysis did not contain sphingosines or free very-long-chain fatty acids. However, our observation that FuB treatment alone did not inhibit ERAD indicates that ceramides are the best candidates because FuB causes accumulation of both very-long-chain fatty acids and sphingosine bases (77). To distinguish between Cer 42:0;2 and Cer 44:0;4, we used previously reported genetic deletions that prevent common hydroxylation of ceramides (fig. S6A). AbA was still effective in inhibiting ERAD even in *scs7Δ* cells unable to catalyze the alpha fatty acid hydroxylation of dihydroceramide or phytoceramides (Fig. 5, A and B, and fig. S6B). In either *sur2Δ* or *scs7Δsur2Δ* cells where hydroxylation of dihydroceramide at the C-4 position to phytoceramide is prevented, AbA was unable to stabilize ERAD substrates (Fig. 5, A and B). These findings support Cer 44:0;4 (alpha-hydroxy-phytoceramide, commonly called ceramide C) as the primary inhibitory lipid rather than Cer 42:0;2.

Next, we manipulated the acyl chain length using yeast 3-keto acyl-CoA (coenzyme A) synthases: Elo1, Elo2, and Elo3. Elo1 catalyzes the elongation of long-chain fatty acids (a fatty acid with 14 to 20 carbons), while Elo2 and Elo3 catalyze the elongation of very-long-chain fatty acids (a fatty acid with 22 or more carbons) and are required for normal sphingolipid formation (Fig. 1A) (80). As a result, *elo2Δ* and *elo3Δ* synthesize sphingolipids with shortened fatty acid moieties. Both *elo2Δ* and *elo3Δ* are viable, but double deletions are synthetically lethal (81). Strains with *elo1Δ* still contain very-long-chain fatty acids (80), and treatment of *elo1Δ* cells with AbA inhibited Hrd1 degradation, as in the wild type (Fig. 5C and fig. S6C). We reasoned that AbA-dependent ERAD inhibition would be abrogated in *elo2Δ* or *elo3Δ* cells lacking an accumulation of very-long-chain ceramides. Somewhat unexpectedly, we observed that AbA treatment only partially impaired Hrd1 degradation in *elo2Δ* or *elo3Δ* cells (Fig. 5C and fig. S6C). Both soluble and integral membrane substrates were degraded in *elo2Δ* and *elo3Δ* cells treated with AbA, supporting a specific role for very-long-chain ceramides in the inhibition of ERAD substrate degradation [CPY* and Erg3 in Fig. 5 (D and E)]. The *elo2Δ* and *elo3Δ* cells were less AbA sensitive compared to wild-type cells (Fig. 5F). When we analyzed the lipidome of *elo3Δ* cells, we found that the overall lipid profiles had notable changes, but Cer 44:0;4 was not detected in our samples (Fig. 5G, fig. S6D, and dataset S2).

To test whether any other very-long-chain fatty acyl chain-containing lipids are likely to be involved in ERAD regulation, we analyzed the subspecies of all quantified lipids that may contain very-long-chain fatty acids including ceramides (≥C42 total), sphingolipids (≥C42 total), phosphatidylinositol (≥C22 from either chain), triacylglycerols (≥C52 total), and cardiolipin (≥C64 total; fig. S6E). Among these lipids, only very-long-chain ceramide showed correlation with ERAD function.

To further test whether Cer 44:0;4 at the ER was required to inhibit ERAD function, we reasoned that ER-localized ceramidases should prevent the AbA-mediated ERAD inhibition. When we overexpressed Flag-tagged versions of the ER-localized ceramidases
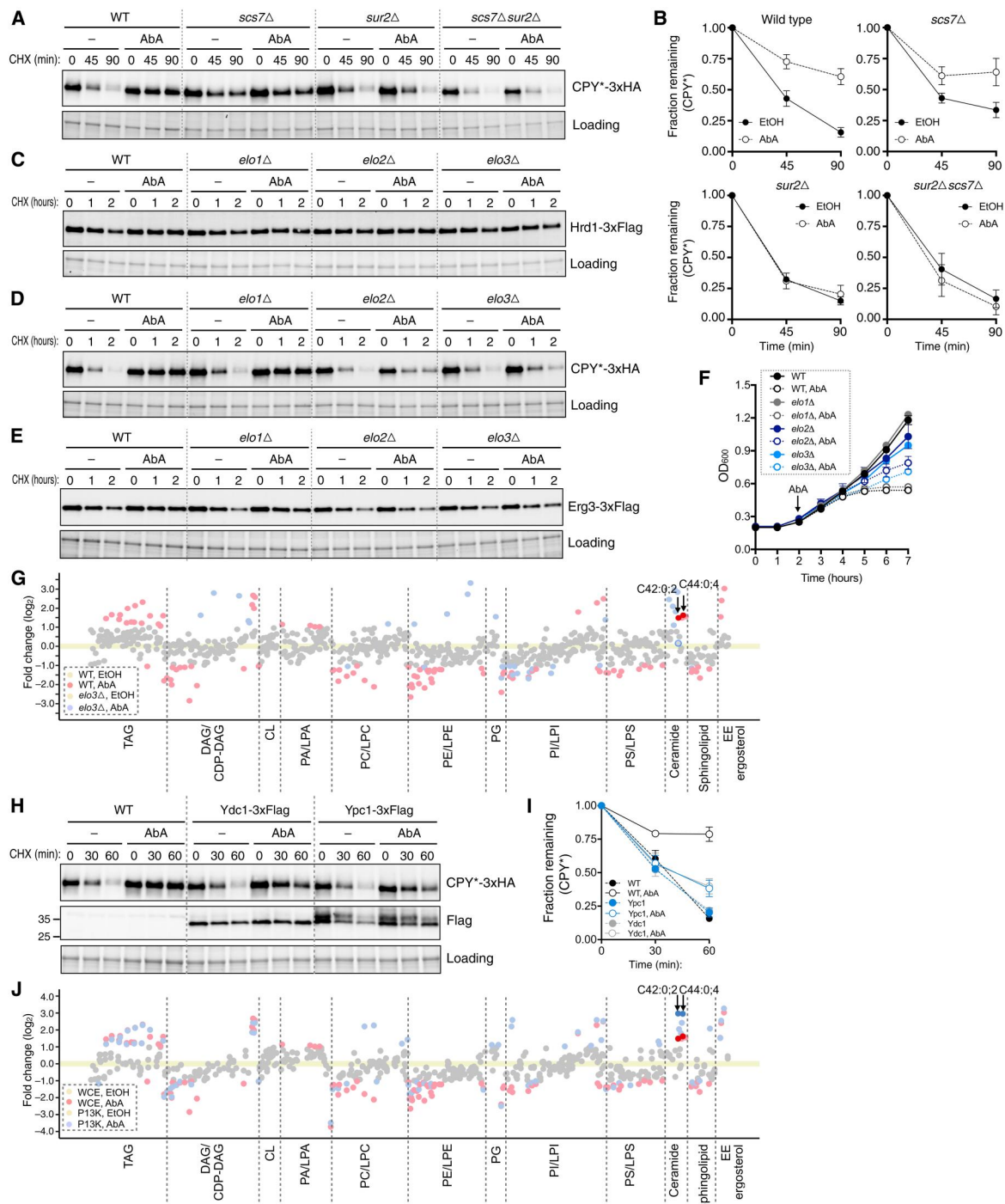
Fig. 5. Very-long-chain ceramides restrict ERAD function. (**A**) Wild-type (WT), *scs7Δ*, *sur2Δ*, or *scs7sur2Δ* cells with chromosomally integrated CPY*-3xHA were pre-treated with AbA (0.5 μg/ml) for 2 hours before cycloheximide chase degradation assay. Total protein was visualized by stain-free dye. (**B**) Quantification of (A). (**C** and **D**) As in (A) but Hrd1-3xFlag and CPY*-3xHA were expressed from centromeric plasmids in wild-type, *elo1Δ*, *elo2Δ*, or *elo3Δ* cells. (**E**) As in (C) but with Erg3-3xFlag. (**F**) Growth assay of wild-type, *elo1Δ*, *elo2Δ*, or *elo3Δ* cells in liquid media. Data are presented as means ± SD from three experiments. (**G**) Comparative lipidomics of wild-type or *elo3Δ* cells treated with ethanol or AbA. Values that are presented as the fold change of two independent biological replicates for 681 lipid subspecies relative to their control (ethanol-treated wild type or *elo3Δ* cells) are shown as dots. Lipids with less than a two-fold change are shown in gray. Lipid subspecies were grouped on the basis of lipid class. Bright red colors indicate C42:0;2 and C44:0;4 from an ERAD-defective group (wild-type cells treated with AbA). A blue-circled gray dot indicates C42:0;2 from ERAD-functional groups (*elo3Δ* cells treated with AbA). (**H**) As in (A) but with wild-type cells containing an empty vector or expressing Ydc1-3xFlag or Ypc1-3xFlag from GPD promoter. AbA was used at 0.25 μg/ml. Total protein was visualized by stain-free dye. (**I**) Quantification of (H). (**J**) As in (G) but with whole-cell extract (WCE) or microsome-enriched fraction (P_{13K}) from wild-type cells treated with ethanol or AbA. Bright red dots, C42:0;2 and C44:0;4 from WCE; blue dots, C42:0;2 and C44:0;4 from P_{13K}. Each immunoblot is representative of at least three independent biological replicates. For each quantification, data from three experiments are presented as means ± SEM. See also fig. S6.

Ydc1 and Ypc1, we found that degradation of CPY* continued normally (Fig. 5, H and I). However, when cells overexpressing Ydc1 or Ypc1 were treated with AbA, CPY* was still degraded.

Next, we tested whether ceramide was accumulated at the ER or within other cellular organelles. We lysed cells by cryogrinding and fractionated the organelles using differential centrifugation. We were unable to completely separate the ER from other organelles but noticed that our 13,000g pellet contained primarily ER (as marked by Erg3-Flag) and plasma membrane (as marked by Pma1) (fig. S6, F and G). With untreated cells, the concentration of Cer 44:0;4 within the 13K pellet was 1.7-fold higher than in the whole-cell lysates, meaning that ceramide is enriched in either the ER or plasma membrane even under "normal" conditions (dataset S3). When treated with AbA, Cer 44:0;4 was 4.3-fold higher than the concentration in the whole-cell extract treated with AbA and 13-fold higher compared to the untreated whole-cell extract, again, demonstrating an enrichment under the conditions used in our study (Fig. 5J and dataset S3). Together, the combination of the $elo2\Delta$, $elo3\Delta$, $sur2\Delta$, and ceramidase data strongly supports that ERAD is specifically inhibited by the accumulation of very-long-chain phytoceramides, likely at the ER.

The ERAD complex properly assembles and ubiquitinates substrates following ceramide accumulation

On the basis of previous work, the Hrd1-centric ERAD process involves a series of steps including substrate recognition, retrotranslocation, ubiquitination, and extraction [or dislocation (36)]. Under normal cellular conditions, substrate recognition and retrotranslocation require the Hrd3, Usa1, and Der1 proteins within the Hrd1 complex. We first tested whether the Hrd1 ERAD complex remained intact following treatment with AbA. Hrd1 was still associated with Hrd3, Usa1 (Fig. 6A), and Der1 (Fig. 6B) and effectively formed an oligomeric complex containing multiple copies of Hrd1 (Fig. 6C), a prerequisite for function (33, 34). Collectively, we concluded that Aur1 inactivation by AbA treatment did not affect Hrd1 complex formation. Next, we examined the levels of total ubiquitination in microsomal membranes (primarily the ER) of cells treated with AbA. In the microsomal pellet (P_{18K}), we observed an increase in the amount of ubiquitination following AbA treatment, while total ubiquitinated proteins in the cytoplasmic fraction (S_{100K}) were similar (Fig. 6D). This result supports the idea that ubiquitination and the associated machineries are intact and functional (Figs. 2 and 3) but leaves the possibilities that ERAD substrates may not be (i) properly retrotranslocated across the ER membrane, (ii) ubiquitinated, (iii) or extracted from the ER into the cytoplasm. Previous reports have demonstrated that autoubiquitination of Hrd1 is critical for retrotranslocation of ERAD-L substrates (26). To test whether AbA treatment alters Hrd1 autoubiquitination, we purified His-tagged Hrd1 from the microsomal membrane under denaturing conditions and subjected the material to SDS-polyacrylamide gel electrophoresis (SDS-PAGE) and immunoblotting with anti-ubiquitin antibodies (Fig. 6E). Somewhat unexpectedly, the level of polyubiquitinated Hrd1 was increased upon AbA treatment, indicating that Hrd1's ubiquitination activity was intact. Because Hrd1 was activated, we next turned our attention to substrate ubiquitination using Erg3, an integral membrane Hrd1 substrate. As with Hrd1, we purified His-tagged Erg3 (Erg3-3xV5-His$_{10}$) under denaturing conditions from the microsomal membranes. Notably, AbA treatment greatly increased ubiquitination of Erg3 in the ER-enriched microsome (Fig. 6F). In summary, AbA treatment does not inhibit Hrd1 activation required to retrotranslocate substrates or Hrd1's ability to ubiquitinate Erg3. However, we already observed that Erg3 was stabilized by AbA treatment (Fig. 2A) and that the ubiquitin proteasome system was intact (Fig. 2, E and F). Therefore, we hypothesized that Hrd1 substrates may not be efficiently extracted from AbA-induced remodeled ER membrane, resulting in the accumulation of ubiquitinated Erg3 in microsomes.

ERAD fails to extract membrane substrates with ceramide accumulation

To examine the levels of cytoplasmic, and extracted, Hrd1 substrates, we developed an assay to follow the extraction of Erg3 (fig. S7A). We lysed the cells by cryogrinding and collected the microsomal (P_{18K}) and cytosolic fractions (S_{100K}) (fig. S7A). The microsomes contained most of the Erg3 and all of the integral membrane ER protein Hrd3, confirming no contamination of membrane proteins in the extracted material (fig. S7B). The supernatant (S_{100K}) contained the cytoplasmic proteins, including the known soluble cytoplasmic protein Pgk1 (Fig. 7A). Erg3 found in the cytoplasmic fraction (S_{100K}) represented fully-extracted Erg3 protein. AbA treatment resulted in a ~40% reduction in cytoplasmic Erg3 [Fig. 7, A (lane 9 versus 10) and B]. Inhibiting protein translation following AbA treatment reduced the level of extracted Erg3 even further, to a 60% reduction of extracted Erg3 [Fig. 7, A (lane 11 versus 12) and B]. The Erg3 protein appeared as a doublet in the cytoplasmic fractions by SDS-PAGE. To test whether this represented an ER-glycosylated form of Erg3, we used peptide N-glycosidase F (PNGase F) treatment and confirmed that the upper band represented the glycosylated form and the lower band was deglycosylated or unglycosylated Erg3 (fig. S7C). The presence of glycosylated Erg3 demonstrated that some of the cytoplasmic Erg3 originated directly from the ER and represented ERAD-extracted protein. Furthermore, the glycosylated Erg3 was endoglycosidase H sensitive, further supporting the direct ER origin of this extracted substrate (fig. S7D). We tested two additional Hrd1 substrates, Erg25 and Erg5, for the ceramide-induced extraction defect (fig. S7, E and F). We observed similar extraction defects under AbA treatment for both Erg25 (Fig. 7, C and D) and Erg5 (fig. S7G). To ensure the fidelity of our extraction assay, we also tested the ER-localized membrane protein Elo1, which is not extracted, and confirmed that it was not found in the cytosolic fractions (Fig. 7C). Collectively, these extraction assays support the idea that ubiquitinated ERAD substrates are trapped in the ER following inefficient extraction into the cytoplasm under conditions of very-long-chain ceramide accumulation, causing their stabilization.

DISCUSSION

In this study, we have illuminated a previously unrecognized mechanism that restricts the activity of the Hrd1-centric ERAD system. Our results provide the first evidence that the ERAD process can be altered by specific lipids within the ER membrane. Using both pharmacological and genetic methods, we demonstrated that accumulation of ceramides inhibited the degradation of ERAD substrates (Figs. 1 to 3). Through lipidomic analysis under multiple experimental conditions, we recognized that the accumulation of saturated very-long-chain ceramides, specifically C44:0;4 alpha-hydroxy-phytoceramide, resulted in inactivation of the Hrd1-ERAD system
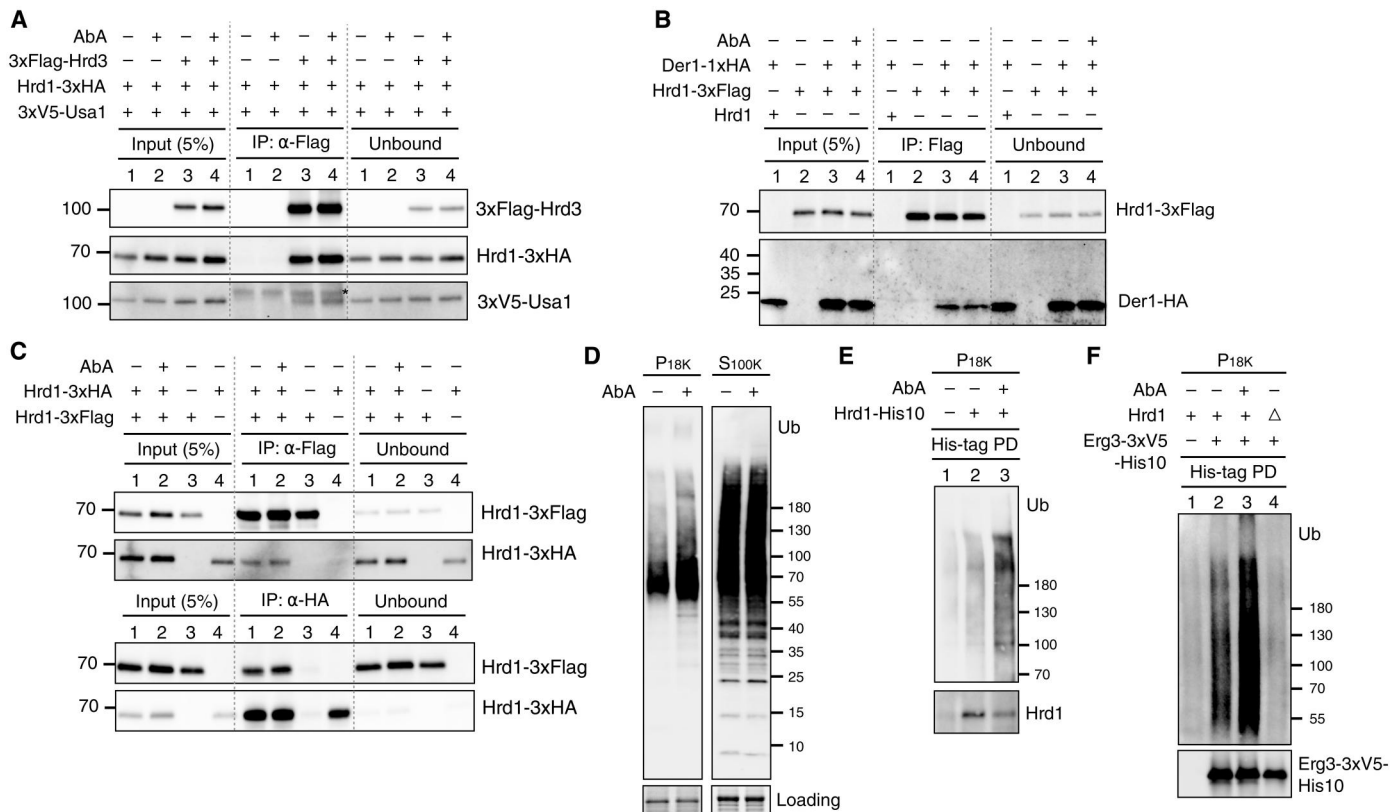
Fig. 6. The ERAD complex assembles and ubiquitinates integral membrane substrates during ceramide accumulation. (**A**) 3xFlag-Hrd3, Hrd1-3xHA, and 3xV5-Usa1 were expressed from their endogenous promoters on centromeric plasmids in *hrd1Δhrd3Δusa1Δ* cells. Microsomal fractions were solubilized; Hrd3 was immuno-precipitated with anti-Flag resin, and samples were analyzed for interacting proteins by immunoblotting. The asterisk indicates a nonspecific cross-reacting band. (**B**) As in (A) but with Hrd1-3xFlag and Der1-HA in *hrd1Δder1Δ* cells. (**C**) As in (A) but with Hrd1-3xFlag and Hrd1-3xHA in *hrd1Δ* cells and immunoprecipitation using either anti-Flag beads (top) or anti-HA antibody (bottom). (**D**) His-tagged Hrd1 (Hrd1-His10) was expressed from a centromeric plasmid in *hrd1Δpdr5Δ* cells. Cells were treated with ethanol or AbA for 2 hours and bortezomib for 30 min prior to cell lysis. The microsomal fraction (P_{18K}) was obtained by centrifugation of the cleared cell lysate at 18,000*g*. The soluble fraction (S_{18K}) was centrifuged at 100,000*g* spin to clear the membranes and obtain the cytosolic fraction (S_{100K}). Samples were analyzed by SDS-PAGE and immunoblotting with anti-ubiquitin antibody, and total protein was visualized using stain-free dye. (**E**) Hrd1-His10–expressing *hrd1Δpdr5Δ* cells were treated with ethanol or AbA for 2 hours before cell lysis. P_{18K} fractions were obtained as described in (D) under denaturing conditions containing 6 M urea. His-tag Dynabeads were added to pull down His-tagged Hrd1 (His-tag PD), and eluted materials were analyzed by SDS-PAGE and immunoblotting with anti-ubiquitin antibody (top) or anti-Hrd1 antibody (bottom). *hrd1Δ* cells with an empty vector were included as a negative control (lane 1). (**F**) As in (E) but with His-tagged Erg3-3xV5-His10 in wild-type or *hrd1Δ* cells. His-tag pulldowns were immunoblotted with anti-ubiquitin antibody (top) or anti-V5 antibody (bottom). Each immunoblot is representative of at least three biological replicates.

(Figs. 4 and 5). By genetically preventing biosynthesis of this satu-rated very-long-chain ceramide or manipulating the levels using ER-localized ceramidases, we were able to confirm this candidate lipid as the central inhibitory molecule (Fig. 5). Accumulation of very-long-chain ceramides specifically prevents the extraction of ERAD substrates from the membrane, although these substrates are ubiquitinated (Figs. 6 and 7).

The essential features of ERAD are highly conserved among eu-karyotes, but the mammalian ERAD system is expected to be far more complicated than that in yeast because of the expanded diver-sity of ERAD components and regulatory mechanisms. We propose that these ceramide-mediated ERAD control mechanics would be conserved in other eukaryotes, including mammals, but a targeted approach is required to validate this idea. Phytoceramides are present within many eukaryotes including both mammals and plants (*82, 83*), and this work provides a basis to test the role of spe-cific ceramide candidates on ERAD activity in other eukaryotes.

Ceramides play diverse roles in cellular functions; they have been recognized as a central structural component of the membrane and a second messenger that mediates cell proliferation, differenti-ation, motility, and death (*84, 85*). Normally, ceramide levels would remain low within the ER [~1 mole percent (mol %)] and may not play much of a regulatory role. However, elevated ceramides are as-sociated with a wide range of pathologies. For example, ER-localized ceramides are elevated in common metabolic conditions including obesity and type 2 diabetes (*60*) and cardiovascular disease (*61*). In-fections including certain lung diseases (*86*), dengue or West Nile viruses (*87*), or nervous system injuries also result in elevated cer-amides (*88*). Many cases of aging or neurodegeneration are corre-lated with ceramide elevation including multiple sclerosis, Alzheimer's disease, and Parkinson's disease (*89*). Impaired ERAD function is also implicated in similar pathologic conditions (*52*). Our results put an interesting twist on the role of ceramides and their effect on ERAD activity in the context of these conditions:
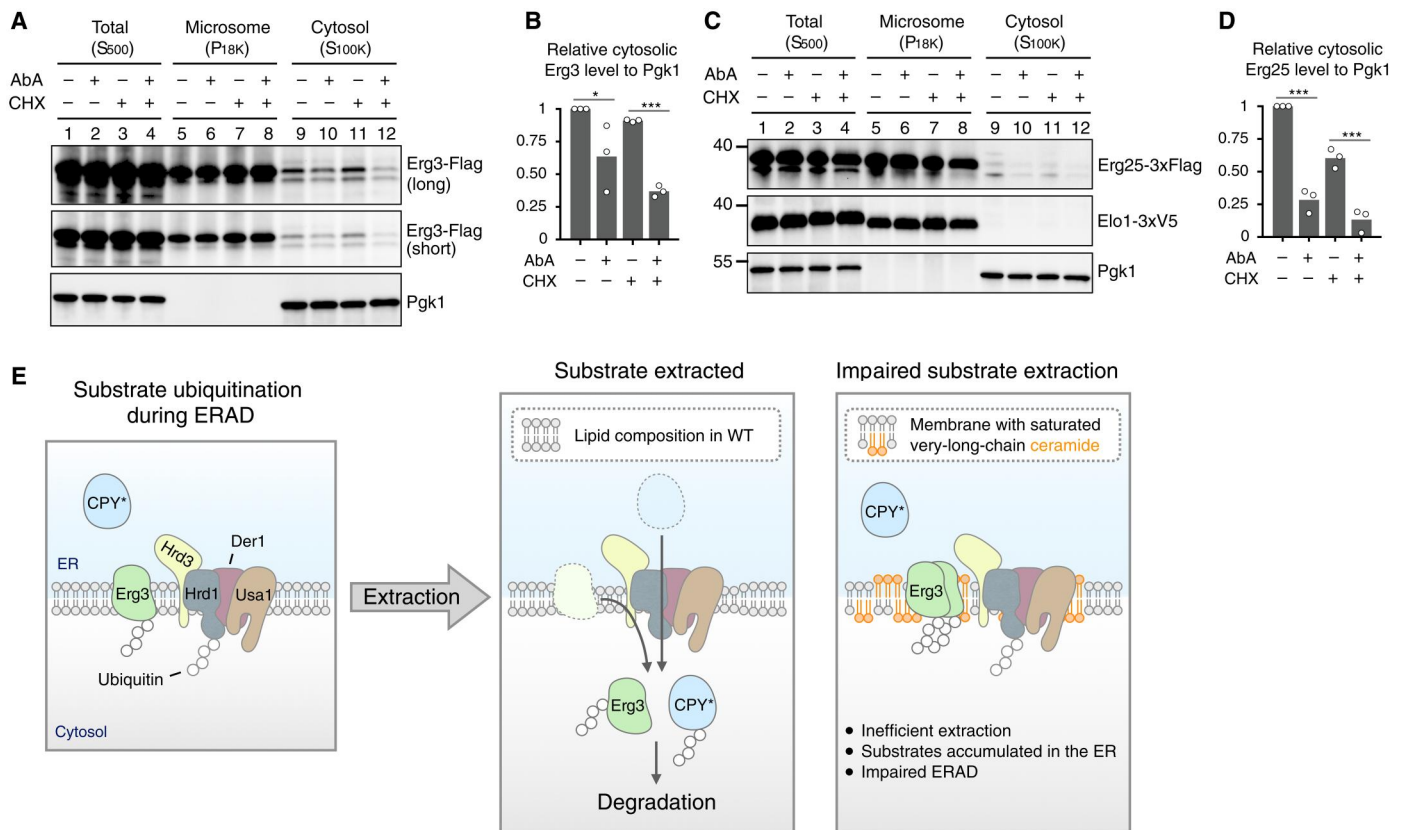
Fig. 7. Ceramide accumulation prevents the ERAD complex from extracting ubiquitinated integral membrane proteins. (**A**) Wild-type cells expressing His-tagged Erg3-3xFlag were pretreated with ethanol or AbA for 2 hours before bortezomib and cycloheximide addition for an additional hour. The unbroken cells were cleared by centrifugation at $500g$ (S_{500}). The microsomal fraction was collected at $18,000g$ (P_{18K}). The cytosol was collected by centrifugation at $100,000g$ (S_{100K}) to clear the remaining membranes . Equal amounts of samples were analyzed by SDS-PAGE and immunoblotting with anti-Flag or anti-Pgk1 antibody. (**B**) The amounts of Erg3 in the P_{18K} and S_{100K} were normalized to their respective Pgk1 levels. Data from three independent experiments are presented as means. P values from two-tailed t tests are indicated as $*P < 0.05$ or $***P < 0.0005$. (**C** and **D**) As in (A) and (B) but with Erg25-3xFlag and Elo1-3xV5. (**E**) A working model for the ERAD system controlled by ceramide in the ER. Left: Hrd1 substrates are targeted for ubiquitination and retrotranslocation during ERAD. Right: Under normal conditions, ubiquitinated Hrd1 substrates are extracted from the membrane and degraded by proteasome in the cytosol. Membrane thinning of the local lipid bilayer may assist ERAD substrate retrotranslocation or extraction. Accumulation of saturated very-long-chain ceramides within the ER membrane prevents ERAD substrate extraction, possibly by affecting local membrane thinning or altering other biophysical properties of the membrane or through specific interactions with protein components. Hrd1 E3 ligase activity is intact, but ubiquitinated substrates are not efficiently extracted from the membrane, resulting in their accumulation in the ER. Each immunoblot is representative of at least three independent biological replicates. See also fig. S7.

reduced ERAD function due to elevated ceramide could be contributing to some of these phenotypes. The fact that saturated very-long-chain phytoceramides are specific ERAD inhibitory molecules makes it possible that biophysical properties play an important role, but the mechanics of how ceramides control ERAD will require further investigation. Because of the specificity of the ceramide that we have identified, it may be more likely that, rather than altering the biophysical properties of the membrane to reduce ERAD function, Cer 44:0;4 is a specific interaction with a protein component in the system. However, testing each of these models will require in vitro reconstitution to dissect the mechanics. First, this will require the development of an assay for the extraction step and later to illuminate the specific role played by the specific ceramides.

Multiple substrates of the ERAD system are known to be regulated by specific lipid species, primarily within the sterol biosynthesis pathway (*65*). To date, these substrates or their "chaperoning"

protein interactions have always been the target of the lipid species controlling their degradation (*6*, *90*). This study provides the first evidence that the composition of the membrane can alter the activity of the Hrd1-ERAD system itself. We have identified a unique link between ERAD function and the sphingolipid biosynthesis pathway. This is particularly interesting because of the crosstalk between the sphingolipid and sterol metabolic pathways; these lipids have biochemical affinity for each other and are co-regulated (*91–93*). In mammals, the sterol regulatory element-binding protein appears to be directly regulated by ceramides (*94*). Our discovery is somewhat reminiscent of previous work that demonstrated that disruption of a fatty acid synthase caused a global disruption in the membrane composition that reduced the degradation of ERAD substrates (*95*). Although it is worth noting that in this previous study, the authors' interpretation was that substrates were never appropriately targeted to the ERAD system because they lacked the appropriate glycosylation state. Even in this example, the lack of

degradation due to elevated cellular lipid was from an effect on ERAD substrates rather than on the activity of ERAD systems themselves (95).

At first glance, the AbA-mediated inhibition of a Golgi-localized IPC synthase enzyme complex leading to the inactivation of the ER-localized ERAD system might seem counterintuitive (see Fig. 1A). However, most ceramides are transported from the ER to the trans-Golgi through nonvesicular transport (96). Because of this, Aur1/Kei1 inactivation would lead to ceramide accumulation not only in the Golgi but also in the ER. We were unable to directly measure the concentration of ceramides in a pure ER fraction. However, within an isolated fraction that contained the ER and plasma membrane (P_{13K}), the ceramides were enriched at least approximately 1.7-fold relative to the untreated control. When cells were treated with AbA, Cer 44:0;4 was increased approximately 4-fold and 13-fold at the P_{13K} relative to an untreated whole-cell lysate. Even if the ceramide was distributed equally between the ER and plasma membrane, this represents a major increase in a relatively uncommon lipid within the compartments. We consider it more likely that the ceramide is located at the ER because the biosynthesis pathway is located at the ER and the inositol phosphosphingolipid phospholipase C, Isc1, that hydrolyzes complex sphingolipid to ceramide and inositol phosphate is localized to the mitochondria and ER (97). For the fractionation procedure, we used an alternate lysis method by cryogrinding to maintain "intact" organelles compared to the standard bead beating procedure. Somewhat unexpectedly, we obtained lower overall ceramide concentrations in cells lysed with this method. It is probably important to note that the entire fractionation procedure for cryogrinding through final fraction collection takes 3 hours, whereas with bead beating, the samples are lysed and immediately snap-frozen. The reduced processing time may account for the differences in absolute ceramide concentrations between samples (overall, about four times lower for the cryo-ground and fractionated cells).

In our standard lipidomic analysis with whole-cell lysates, we quantified total ceramides in a range from 0.2 to 0.45 mol % in untreated wild-type cells and maxed out at 1.3 mol % with the AbA and FuB treatment (fig. S3, C and E). These results are consistent with previous reports of ceramides at near 1 mol % (80). In the P_{13K}, we observed an ~eight-fold increase in ceramide when comparing the untreated and AbA-treated samples, although these actual measurements were 1.1 mol % in the mixed ER plasma membrane fraction (Fig. 5J and dataset S3). By projecting the enrichment of ceramides at the ER based on our fractionation results to more standard measurements of ceramide levels [assuming 0.5 to 1 mol % (80)], we would observe marked changes that could correspond to 4 to 8 mol % total ceramide at the ER. In addition, lipid distributions can be heterogeneous, even in the ER (98), so local concentrations of these ceramides could be even higher. Accumulation of as little as 2 to 5% phytoceramide in model membranes remodels local membrane environments into more highly rigid gel domains (99, 100). Our treatments could alter the biophysical properties of the ER membrane and could induce a ceramide-enriched highly ordered membrane platform that somehow restricts ERAD function. Note that Hrd1 autoubiquitination and Hrd1-dependent substrate ubiquitination are still intact, meaning that substrates were not completely physically separated from Hrd1 (Fig. 6, E and F). On the other hand, we have not observed ubiquitinated ERAD-L substrates accumulating within the ER membrane. Unfortunately, it is unclear whether this is a failure of the assay or whether this result reflects the biology of the system, meaning that retrotranslocation of CPY* to the cytoplasmic side of the membrane is inhibited. Our biochemical studies to examine the role of ceramide on ERAD suggest that elevated ceramide does not alter Hrd1 core complex formation or its E3 ubiquitin ligase activity, but it substantially hampers membrane substrate extraction from the ER membrane to the cytoplasm (Fig. 7, A to D). Recent work has proposed that membrane "thinning" of the local lipid bilayer might be the principle used to reduce the energy barrier to assist ERAD substrate retrotranslocation or extraction (23, 46, 47). If lipid thinning is a central principle for ERAD function, saturated very-long-chain ceramides accumulating in the ER would affect local membrane thinning required by the ERAD system for function (40, 101). Alternatively, the remodeled lipid membrane compositions may affect the function of specific ERAD proteins or the recruitment of key factors required for retrotranslocation and extraction, such as the ubiquitin chain linkages, UBX proteins, or Cdc48 and its cofactors. In ERAD, the specific mechanics of how ceramides prevent the extraction of substrates requires further investigation and will likely require an in vitro reconstituted system to understand the mechanics of inhibition by the very-long-chain ceramides for both soluble and integral membrane substrates (25, 26).

This work supports an interesting role for feedback between the lipid bilayer and ERAD. The ERAD complex exists within the ER lipid bilayer and controls the degradation of many lipid biosynthetic enzymes in the related sterol synthesis pathway. We propose that in certain cases, the ERAD systems would be controlled by the composition of the ER membrane. While accumulation of ceramide can result in a complete inactivation of the Hrd1-ERAD system, it is likely that in many other circumstances, there would be a smaller effect on ERAD that would either reduce the activity or could alter the specificity of the system. Here, we have implicated ceramide in the regulation of ERAD, but more broadly, our work raises the possibility that ERAD function could be modulated by the presence or absence of other lipid species that remain to be identified.

MATERIALS AND METHODS
Yeast strains and plasmids
Deletion strains used in this study were purchased from Horizon Discovery Ltd. and are derivatives of BY4741 (MATa his3Δ1 leu2Δ0 met15Δ0 ura3Δ0) or BY4742 (MATα his3Δ1 leu2Δ0 lys2Δ0 ura3Δ0). Triple deletion strains (hrd1Δhrd3Δusa1Δ) were generated by crossing a hrd1Δ and hrd3Δusa1Δ (28), sporulating the diploid, and screening by polymerase chain reaction (PCR) for the hrd1Δhrd3Δusa1Δ. The elo1Δ, elo2Δ, elo3Δ, scs7Δ, and sur2Δ haploid cells were generated by sporulating respective diploid cells from the yeast heterozygous diploid knockout collection (Horizon Discovery). The scs7Δsur2Δ strain was generated by crossing the scs7Δ and sur2Δ strains, sporulating the resulting diploid, and screening the appropriate loci by PCR. The temperature-sensitive kei1-1 cells were generated on the basis of a previously reported mutant (76). Briefly, the KEI1/kei1::kanR heterozygous diploid cells (Horizon Discovery) were transformed with the PCR product containing kei1-1 and hygromycin-resistant cassette amplified from pJH70. After selection and sporulation, genotypes were verified by PCR and sequencing. For a list of yeast strains used in

this study, see table S1. Plasmids were constructed using standard restriction cloning or NEB HiFi assembly (New England Biolabs). All plasmids used in this study were either centromeric (102) or custom integrating plasmids. Yeast plasmids were transformed using the lithium acetate/polyethylene glycol (LiAc/PEG) method (103). For a list of plasmids used in this study, see table S2.

Degradation assays

Cycloheximide chase degradation assays were performed as described previously (104) with the following modifications. Cells were grown to mid-log phase [0.4 to 0.7 optical density at 600 nm (OD_{600})/ml] in synthetic dropout media. The cells were pelleted at 2000g for 5 min and resuspended to 2 OD_{600}/ml in fresh media. At time "0 min" or "0 hour," the culture was supplemented with cycloheximide (50 μg/ml), and an aliquot was collected and centrifuged as above. The supernatant was removed, and the cell pellet was either flash-frozen in liquid N_2 or resuspended in lysis buffer. The remaining culture was incubated at 30°C with samples taken as indicated.

Cell pellets were resuspended in lysis buffer [10 mM Mops (pH 6.8), 1% SDS, 8 M urea, 10 mM EDTA, and fresh protease inhibitors] at 20 OD_{600}/ml with an equivalent volume of acid-washed glass beads (0.1 mm, Bio-Spec). Cells were vortexed for 2 min before an equal volume of urea sample buffer [125 mM tris (pH 6.8), 4% SDS, 8 M urea, and 10% β-mercaptoethanol] was added and mixed. The samples were incubated at 65°C for 5 min before they were separated in SDS-PAGE, transferred to a polyvinylidene difluoride (PVDF) membrane, immunoblotted with antibodies [anti-DYKDDDK, GenScript; anti-hemagglutinin (HA), Roche; anti-V5, GenScript; anti-PAP (Peroxidase Anti-Peroxidase soluble complex), Sigma-Aldrich; horseradish peroxidase–linked ECL rabbit immunoglobulin G (IgG) and mouse IgG, Amersham; goat anti-mouse IgG Alexa800, Invitrogen], and detected by chemiluminescence ECL Select Western blotting detection reagent (Amersham) on a ChemiDoc MP (Bio-Rad). For quantification of the immunoblot band intensities, band intensities were normalized on the basis of the total protein in the sample quantified within the same gels using Bio-Rad Stain-Free Dye Imaging Technology (stain-free dye) or by normalization to the intensity of anti-Pgk1 (Invitrogen).

Detection of ubiquitination in vivo

Denaturing pulldowns of Hrd1 or Erg3 were performed as described previously (26) with the following modifications. Cells (100 OD) with a centromeric plasmid containing Hrd1-His10 expressed from an endogenous Hrd1 promoter were grown to mid-log phase and resuspended in R buffer [50 mM tris (pH 7.4) and 300 mM NaCl] with protease inhibitors, 1 mM phenylmethylsulfonyl fluoride [PMSF (Sigma-Aldrich)] and 1.5 μM pepstatin A (Adipogen Life Sciences), 5 μM bortezomib [to inhibit proteasomal degradation (ApexBio Technology)], and 5 mM N-ethylmaleimide (to inhibit deubiquitinating enzymes). For Erg3 pulldowns, Erg3-3xV5-His10 bearing an endogenous Erg3 promoter was integrated into the *leu2* locus in wild-type or *hrd1Δ* cells. The cell resuspension was snap-frozen drop by drop in liquid N_2 to form small yeast "balls" and cryogenically ground using a SPEX 6875D freezer/mill (grinding rate: 5 cycles per second, five cycles; SPEX SamplePrep). The frozen cell powder was thawed on ice and resuspended in 1 ml of L buffer [50 mM tris (pH 7.4), 300 mM NaCl, and 6 M urea] with

protease inhibitors, 1 mM PMSF and 1.5 μM pepstatin, 5 μM bortezomib, and 5 mM N-ethylmaleimide. The lysates were centrifuged at 18,000g for 10 min. The microsome-enriched pellets (P_{18K}) were solubilized in the LT buffer [50 mM tris (pH 7.4), 300 mM NaCl, 6 M urea, and 1.5% Triton X-100 (Anatrace) final] with protease inhibitors and 25 mM imidazole for 1 hour at 4°C. His-tag Dynabeads (Life Technologies) were added (20 μl per 100 OD of cells) and incubated for an additional 1 hour. The beads were washed six to seven times with 1× volumes of LT buffer. Hrd1-His10 was eluted with E buffer [50 mM tris (pH 7.4), 300 mM NaCl, 6 M urea, 0.5% Triton X-100, and 400 mM imidazole]. The samples were analyzed by SDS-PAGE and immunoblotting with anti-Hrd1, anti-V5, or anti-ubiquitin antibodies (clone P4D1, Santa Cruz Biotechnology).

Detection of cytosolic ERAD substrates

Wild-type cells with chromosomally integrated Erg3 promoter-Erg3-3xFlag at the *leu2* locus or Erg5 promoter-Erg5-3xFlag or Erg25 promoter-Erg25-3xFlag at the *his3* locus were grown to mid-log phase and lysed in R buffer [50 mM tris (pH 7.4) and 300 mM NaCl] with protease inhibitors and 5 μM bortezomib using a cryogenic freezer mill as described above. The frozen cell powder was thawed on ice and resuspended in 1 ml of the R buffer [50 mM tris (pH 7.4) and 300 mM NaCl] with protease inhibitors and 5 μM bortezomib. The lysates were centrifuged at 500g for 5 min to clear lysates. The supernatant (S_{500}) was collected and recentrifuged at 18,000g for 10 min. The microsome-enriched pellets (P_{18K}) were washed with 1 ml of the R buffer containing protease inhibitors and bortezomib twice and then solubilized in the RT buffer [50 mM tris (pH 7.4), 300 mM NaCl, and 1.5% Triton X-100 final] with protease inhibitors and 5 μM bortezomib for 1 hour at 4°C. The supernatant after centrifugation at 18,000g (S_{18K}) was collected and ultracentrifuged for 1 hour at 50,000 rpm (112,000g) in a Beckman TLA55 rotor. The supernatant was recentrifuged at 112,000g to eliminate contaminating proteins (S_{100K}). The P_{18K} and S_{100K} were analyzed by SDS-PAGE and immunoblotting with the appropriate antibodies.

Immunoprecipitation of Hrd1 and interacting partners

Cells with centromeric plasmids bearing a combination of Hrd1-3xHA, 3xFlag-Hrd3, and Usa1-3xHA under endogenous promoters were grown to mid-log phase; pelleted; resuspended in buffer [25 mM tris (pH 7.4) and 150 mM NaCl] with protease inhibitors, 1 mM PMSF, and 1.5 μM pepstatin; and flash-frozen in liquid nitrogen to form yeast balls before cryogenic lysis using freezer/mill (SPEX SamplePrep). Cell powders were thawed on ice and centrifuged at 18,000g for 10 min to collect the microsomes. The P_{18K} pellets were resolubilized in lysis buffer [25 mM tris (pH 7.4), 150 mM NaCl, and 1% digitonin (high purity, Calbiochem)] with protease inhibitors for 1 hour at 4°C. Input samples were taken, and 7.5 ODs of solubilized proteins were diluted 1:5 for final 0.2% digitonin, mixed with 20 μl (40 μl slurry) of anti-Flag M2 magnetic beads (Sigma-Aldrich), and rolled for 3 hours at 4°C. The bound proteins were washed six to seven times with 1× volume of IP buffer [25 mM tris (pH 7.4), 150 mM NaCl, and 0.2% digitonin] and eluted with 2× SDS-PAGE sample buffer. The samples were analyzed by SDS-PAGE and immunoblotting with anti-Flag and anti-V5 antibodies with the inputs loaded at 5%. For coimmunoprecipitation of Hrd1 and Der1, *hrd1Δder1Δ* cells with chromosomally integrated Hrd1-3xFlag at the *his3* locus with centromeric plasmids bearing Der1-

HA driven by its endogenous promoter were used. Immunoprecipitation was performed as above for Hrd3 and Usa1 but with decyl maltose neopentyl glycol [DMNG (Anatrace)] instead of digitonin.

Flow cytometry

Cells expressing the *URA3* integrating UPR reporter (4xUPRE-*CYC1*promoter_GFPfast_*CYC1*terminator) with the indicated plasmids were grown to mid-log phase in synthetic dropout media. The cells were treated with AbA (1 μg/ml), 2 mM DTT, or 0.1% ethanol (vehicle control) and grown in glassware. At indicated times after treatment, cells were taken pelleted in a 96-well plate washed with ice-cold phosphate-buffered saline [PBS; 137 mM NaCl, 2.7 mM KCl, 10 mM sodium phosphate buffer, and 1.8 mM KH_2PO_4 (pH 7.4)] and then resuspended in PBS containing the viability dye Sytox Blue (Invitrogen) at 1 μM. Cells were kept on ice before flow cytometry using a MACSQuant VYB flow cytometer (Miltenyi Biotec). The collected cells were analyzed using forward/side scatter to identify single cells, and Sytox Blue fluorescence was used to exclude dead cells. GFP fluorescence was measured from the 488-nm laser with a 525-nm/50-nm band-pass filter set, while Sytox Blue fluorescence was measured from the 405-nm laser with a 450-nm/50-nm band-pass filter set. Data were analyzed and figures were generated using FlowJo V10.7.1 (FlowJo LLC).

Lipid extraction for mass spectrometry–based lipidomic analysis

To prepare samples for whole-cell lipidomic analysis, 20 OD_{600} of the indicated yeast cells were lysed by bead beating with 0.5-mm-diameter borosilicate beads (BioSpec Products) for 10 min at 4°C (in Fig. 4). For the whole-cell and ER-enriched microsomes used for lipidomic analysis in Fig. 5, cells were lysed by cryogrinding and fractionated to separate organelles using differential centrifugation as described above in the "Detection of cytosolic ERAD substrates" section with a few modifications. Briefly, wild-type cells with chromosomally integrated Erg3-3xFlag expressed from its endogenous promoter, at the *leu2* locus, were grown to mid-log phase (0.5 to 1.0 OD_{600}/ml). Cells (200 OD_{600}) were resuspended at 130 to 140 OD_{600}/ml in Dulbecco's PBS (D-PBS) and lysed using a cryogenic freezer mill. About 40 OD_{600} of the cell lysate was collected as the whole-cell fraction for lipidomic analysis. About 160 OD_{600} of the cell lysate was thawed on ice and centrifuged at 1500*g* for 5 min at 4°C. The resulting pellet was collected as the $P_{1.5K}$. The 1.5K supernatant was centrifuged twice more, and the resulting supernatant ($S_{1.5K}$) was carried to the next step. The supernatant was centrifuged at 13,000*g* for 10 min at 4°C. The resulting microsome-enriched pellet (P_{13K}) was resuspended in one-half volume of D-PBS and recentrifuged at 13,000*g* for 10 min at 4°C, and this was repeated a total of three times. The 13K supernatant was centrifuged at 100,000*g*, and the pellet (P_{100K}) and supernatant (S_{100K}) were collected. The P_{13K} was resuspended into D-PBS at a protein concentration of 0.2 mg/ml for lipidomic analysis. Following the differential centrifugation, the fractions were analyzed by SDS-PAGE and immunoblotting with anti-Vma2 (A-6427, Invitrogen), anti-Pma1 (MA1-91567, Invitrogen), anti-porin (459500, Invitrogen), and anti-Tul1 (gift from P. Espenshade). Mass spectrometry (MS)–based lipid analysis was performed by Lipotype GmbH (Dresden, Germany) as described (*80*, *105*). Lipids were extracted using a two-step chloroform/methanol procedure (*80*). Samples were spiked with internal lipid standard mixture containing the following: CDP-DAG 17:0/18:1, ceramide 18:1;2/17:0 (Cer), diacylglycerol 17:0/17:0 (DAG), lysophosphatidate 17:0 (LPA), lyso-phosphatidylcholine 12:0 (LPC), lysophosphatidylethanolamine 17:1 (LPE), lyso-phosphatidylinositol 17:1 (LPI), lysophosphatidylserine 17:1 (LPS), phosphatidate 17:0/14:1 (PA), phosphatidylcholine 17:0/14:1 (PC), phosphatidylethanolamine 17:0/14:1 (PE), phosphatidylglycerol 17:0/14:1 (PG), phosphatidylinositol 17:0/14:1 (PI), phosphatidylserine 17:0/14:1 (PS), ergosterol ester 13:0 (EE), triacylglycerol 17:0/17:0/17:0 (TAG), IPC 44:0;2, MIPC 44:0;2, and M(IP)$_2$C 44:0;2. After extraction, the organic phase was transferred to an infusion plate and dried in a speed vacuum concentrator. For the first step, dry extract was resuspended in 7.5 mM ammonium acetate in chloroform/methanol/propanol (1:2:4, v/v/v), and for the second step, dry extract was resuspended in 33% ethanol solution of methylamine in chloroform/methanol (0.003:5:1, v/v/v). All liquid handling steps were performed using the Hamilton Robotics STARlet robotic platform with the Anti Droplet Control feature for organic solvent pipetting.

MS data acquisition

Samples were analyzed by direct infusion on a Q Exactive mass spectrometer (Thermo Scientific) equipped with a TriVersa Nano-Mate ion source (Advion Biosciences). Samples were analyzed in both positive and negative ion modes with a resolution of $Rm/z = 200 = 280,000$ for MS and $Rm/z = 200 = 17,500$ for MS/MS experiments, in a single acquisition. MS/MS was triggered by an inclusion list encompassing corresponding MS mass ranges scanned in 1-Da increments (*106*). Both MS and MS/MS data were combined to monitor EE, DAG, and TAG ions as ammonium adducts; PC as an acetate adduct; and CL, PA, PE, PG, PI, and PS as deprotonated anions. MS only was used to monitor LPA, LPE, LPI, LPS, IPC, MIPC, and M(IP)$_2$C as deprotonated anions; Cer and LPC as acetate adducts; and ergosterol as protonated ion of an acetylated derivative (*107*).

Lipidomic data analysis and postprocessing

Data were analyzed by Lipotype GmbH (Dresden, Germany) with an in-house developed lipid identification software based on LipidXplorer (*108*, *109*). Data postprocessing and normalization were performed using an in-house developed data management system. Only lipid identifications with a signal-to-noise ratio >5 and a signal intensity five-fold higher than those in corresponding blank samples were considered for further data analysis.

Supplementary Materials

This PDF file includes:
Figs. S1 to S7
Tables S1 and S2

Other Supplementary Material for this manuscript includes the following:
Datasets S1 to S3

View/request a protocol for this paper from *Bio-protocol*.

REFERENCES AND NOTES

1. N. Berner, K. R. Reutter, D. H. Wolf, Protein quality control of the endoplasmic reticulum and ubiquitin-proteasome-triggered degradation of aberrant proteins: Yeast pioneers the path. *Annu. Rev. Biochem.* **87**, 751–782 (2018).

2. G. M. Preston, J. L. Brodsky, The evolving role of ubiquitin modification in endoplasmic reticulum-associated degradation. *Biochem. J.* **474**, 445–469 (2017).

3. J. E. Vance, Phospholipid synthesis and transport in mammalian cells. *Traffic* **16**, 1–18 (2015).

4. S. Lev, Nonvesicular lipid transfer from the endoplasmic reticulum. *Cold Spring Harb. Perspect. Biol.* **4**, a013300 (2012).

5. R. Christiano, N. Nagaraj, F. Frohlich, T. C. Walther, Global proteome turnover analyses of the yeasts S. cerevisiae and S. pombe. *Cell Rep.* **9**, 1959–1965 (2014).

6. M. M. Schumacher, R. A. DeBose-Boyd, Posttranslational regulation of HMG CoA reductase, the rate-limiting enzyme in synthesis of cholesterol. *Annu. Rev. Biochem.* **90**, 659–679 (2021).

7. M. A. Surma, C. Klose, D. Peng, M. Shales, C. Mrejen, A. Stefanko, H. Braberg, D. E. Gordon, D. Vorkel, C. S. Ejsing, R. Farese Jr., K. Simons, N. J. Krogan, R. Ernst, A lipid E-MAP identifies Ubx2 as a critical regulator of lipid saturation and lipid bilayer stress. *Mol. Cell* **51**, 519–530 (2013).

8. O. Foresti, A. Ruggiano, H. K. Hannibal-Bach, C. S. Ejsing, P. Carvalho, Sterol homeostasis requires regulated degradation of squalene monooxygenase by the ubiquitin ligase Doa10/Teb4. *eLife* **2**, e00953 (2013).

9. O. Foresti, V. Rodriguez-Vaello, C. Funaya, P. Carvalho, Quality control of inner nuclear membrane proteins by the Asi complex. *Science* **346**, 751–755 (2014).

10. L. A. Jaenicke, H. Brendebach, M. Selbach, C. Hirsch, Yos9p assists in the degradation of certain nonglycosylated proteins from the endoplasmic reticulum. *Mol. Biol. Cell* **22**, 2937–2945 (2011).

11. T. M. Buck, X. Zeng, P. S. Cantrell, R. T. Cattley, Z. Hasanbasri, M. E. Yates, D. Nguyen, N. A. Yates, J. L. Brodsky, The capture of a disabled proteasome identifies Erg25 as a substrate for endoplasmic reticulum associated degradation. *Mol. Cell. Proteomics* **19**, 1896–1909 (2020).

12. M. Molinari, ER-phagy responses in yeast, plants, and mammalian cells and their crosstalk with UPR and ERAD. *Dev. Cell* **56**, 949–966 (2021).

13. P. Carvalho, V. Goder, T. A. Rapoport, Distinct ubiquitin-ligase complexes define convergent pathways for the degradation of ER proteins. *Cell* **126**, 361–373 (2006).

14. G. Huyer, W. F. Piluek, Z. Fansler, S. G. Kreft, M. Hochstrasser, J. L. Brodsky, S. Michaelis, Distinct machinery is required in Saccharomyces cerevisiae for the endoplasmic reticulum-associated degradation of a multispanning membrane protein and a soluble luminal protein. *J. Biol. Chem.* **279**, 38369–38378 (2004).

15. A. Khmelinskii, E. Blaszczak, M. Pantazopoulou, B. Fischer, D. J. Omnus, G. Le Dez, A. Brossard, A. Gunnarsson, J. D. Barry, M. Meurer, D. Kirrmaier, C. Boone, W. Huber, G. Rabut, P. O. Ljungdahl, M. Knop, Protein quality control at the inner nuclear membrane. *Nature* **516**, 410–413 (2014).

16. S. Vashist, D. T. Ng, Misfolded proteins are sorted by a sequential checkpoint mechanism of ER quality control. *J. Cell Biol.* **165**, 41–52 (2004).

17. R. Swanson, M. Locher, M. Hochstrasser, A conserved ubiquitin ligase of the nuclear envelope/endoplasmic reticulum that functions in both ER-associated and Matalpha2 repressor degradation. *Genes Dev.* **15**, 2660–2674 (2001).

18. N. W. Bays, S. K. Wilhovsky, A. Goradia, K. Hodgkiss-Harlow, R. Y. Hampton, HRD4/NPL4 is required for the proteasomal processing of ubiquitinated ER proteins. *Mol. Biol. Cell* **12**, 4114–4128 (2001).

19. E. Jarosch, C. Taxis, C. Volkwein, J. Bordallo, D. Finley, D. H. Wolf, T. Sommer, Protein dislocation from the ER requires polyubiquitination and the AAA-ATPase Cdc48. *Nat. Cell Biol.* **4**, 134–139 (2002).

20. E. Rabinovich, A. Kerem, K. U. Frohlich, N. Diamant, S. Bar-Nun, AAA-ATPase p97/Cdc48p, a cytosolic chaperone required for endoplasmic reticulum-associated protein degradation. *Mol. Cell. Biol.* **22**, 626–634 (2002).

21. Y. Ye, H. H. Meyer, T. A. Rapoport, The AAA ATPase Cdc48/p97 and its partners transport proteins from the ER into the cytosol. *Nature* **414**, 652–656 (2001).

22. R. G. Gardner, G. M. Swarbrick, N. W. Bays, S. R. Cronin, S. Wilhovsky, L. Seelig, C. Kim, R. Y. Hampton, Endoplasmic reticulum degradation requires lumen to cytosol signaling. Transmembrane control of Hrd1p by Hrd3p. *J. Cell Biol.* **151**, 69–82 (2000).

23. X. Wu, M. Siggel, S. Ovchinnikov, W. Mi, V. Svetlov, E. Nudler, M. Liao, G. Hummer, T. A. Rapoport, Structural basis of ER-associated protein degradation mediated by the Hrd1 ubiquitin ligase complex. *Science* **368**, eaaz2449 (2020).

24. V. Denic, E. M. Quan, J. S. Weissman, A luminal surveillance complex that selects misfolded glycoproteins for ER-associated degradation. *Cell* **126**, 349–359 (2006).

25. A. Stein, A. Ruggiano, P. Carvalho, T. A. Rapoport, Key steps in ERAD of luminal ER proteins reconstituted with purified components. *Cell* **158**, 1375–1388 (2014).

26. R. D. Baldridge, T. A. Rapoport, Autoubiquitination of the Hrd1 ligase triggers protein retrotranslocation in ERAD. *Cell* **166**, 394–407 (2016).

27. R. Y. Hampton, R. G. Gardner, J. Rine, Role of 26S proteasome and HRD genes in the degradation of 3-hydroxy-3-methylglutaryl-CoA reductase, an integral endoplasmic reticulum membrane protein. *Mol. Biol. Cell* **7**, 2029–2044 (1996).

28. B. G. Peterson, M. L. Glaser, T. A. Rapoport, R. D. Baldridge, Cycles of autoubiquitination and deubiquitination regulate the ERAD ubiquitin ligase Hrd1. *eLife* **8**, (2019).

29. V. Vasic, N. Denkert, C. C. Schmidt, D. Riedel, A. Stein, M. Meinecke, Hrd1 forms the retrotranslocation pore regulated by auto-ubiquitination and binding of misfolded proteins. *Nat. Cell Biol.* **22**, 274–281 (2020).

30. S. Schoebel, W. Mi, A. Stein, S. Ovchinnikov, R. Pavlovicz, F. DiMaio, D. Baker, M. G. Chambers, H. Su, D. Li, T. A. Rapoport, M. Liao, Cryo-EM structure of the protein-conducting ERAD channel Hrd1 in complex with Hrd3. *Nature* **548**, 352–355 (2017).

31. M. Mehnert, T. Sommer, E. Jarosch, Der1 promotes movement of misfolded proteins through the endoplasmic reticulum membrane. *Nat. Cell Biol.* **16**, 77–86 (2014).

32. R. Gauss, E. Jarosch, T. Sommer, C. Hirsch, A complex of Yos9p and the HRD ligase integrates endoplasmic reticulum quality control into the degradation machinery. *Nat. Cell Biol.* **8**, 849–854 (2006).

33. P. Carvalho, A. M. Stanley, T. A. Rapoport, Retrotranslocation of a misfolded luminal ER protein by the ubiquitin-ligase Hrd1p. *Cell* **143**, 579–591 (2010).

34. S. C. Horn, J. Hanna, C. Hirsch, C. Volkwein, A. Schutz, U. Heinemann, T. Sommer, E. Jarosch, Usa1 functions as a scaffold of the HRD-ubiquitin ligase. *Mol. Cell* **36**, 782–793 (2009).

35. S. Neal, P. A. Jaeger, S. H. Duttke, C. Benner, C. K. Glass, T. Ideker, R. Y. Hampton, The Dfm1 derlin is required for ERAD retrotranslocation of integral membrane proteins. *Mol. Cell* **69**, 306–320.e4 (2018).

36. V. Dederer, M. K. Lemberg, Transmembrane dislocases: A second chance for protein targeting. *Trends Cell Biol.* **31**, 898–911 (2021).

37. H. J. Kaiser, A. Orlowski, T. Rog, T. K. Nyholm, W. Chai, T. Feizi, D. Lingwood, I. Vattulainen, K. Simons, Lateral sorting in model membranes by cholesterol-mediated hydrophobic matching. *Proc. Natl. Acad. Sci. U.S.A.* **108**, 16628–16633 (2011).

38. F. X. Contreras, A. M. Ernst, P. Haberkant, P. Bjorkholm, E. Lindahl, B. Gonen, C. Tischer, A. Elofsson, G. von Heijne, C. Thiele, R. Pepperkok, F. Wieland, B. Brugger, Molecular recognition of a single sphingolipid species by a protein's transmembrane domain. *Nature* **481**, 525–529 (2012).

39. P. A. Janmey, P. K. Kinnunen, Biophysical properties of lipids and dynamic membranes. *Trends Cell Biol.* **16**, 538–546 (2006).

40. S. Chiantia, N. Kahya, J. Ries, P. Schwille, Effects of ceramide on liquid-ordered domains investigated by simultaneous AFM and FCS. *Biophys. J.* **90**, 4500–4508 (2006).

41. A. Romanauska, A. Kohler, The inner nuclear membrane is a metabolically active territory that generates nuclear lipid droplets. *Cell* **174**, 700–715.e18 (2018).

42. R. Covino, G. Hummer, R. Ernst, Integrated functions of membrane property sensors and a hidden side of the unfolded protein response. *Mol. Cell* **71**, 458–467 (2018).

43. H. Y. Wang, S. Bharti, I. Levental, Membrane heterogeneity beyond the plasma membrane. *Front. Cell Dev. Biol.* **8**, 580814 (2020).

44. S. Urban, M. S. Wolfe, Reconstitution of intramembrane proteolysis in vitro reveals that pure rhomboid is sufficient for catalysis and specificity. *Proc. Natl. Acad. Sci. U.S.A.* **102**, 1883–1888 (2005).

45. A. J. B. Kreutzberger, M. Ji, J. Aaron, L. Mihaljevic, S. Urban, Rhomboid distorts lipids to break the viscosity-imposed speed limit of membrane diffusion. *Science* **363**, eaao0076 (2019).

46. A. Nejatfard, N. Wauer, S. Bhaduri, A. Conn, S. Gourkanti, N. Singh, T. Kuo, R. Kandel, R. E. Amaro, S. E. Neal, Derlin rhomboid pseudoproteases employ substrate engagement and lipid distortion to enable the retrotranslocation of ERAD membrane substrates. *Cell Rep.* **37**, 109840 (2021).

47. X. Wu, T. A. Rapoport, Translocation of proteins through a distorted lipid bilayer. *Trends Cell Biol.* **31**, 473–484 (2021).

48. C. J. Guerriero, J. L. Brodsky, The delicate balance between secreted protein folding and endoplasmic reticulum-associated degradation in human physiology. *Physiol. Rev.* **92**, 537–576 (2012).

49. F. R. Maxfield, I. Tabas, Role of cholesterol and lipid organization in disease. *Nature* **438**, 612–621 (2005).

50. U. Ozcan, Q. Cao, E. Yilmaz, A. H. Lee, N. N. Iwakoshi, E. Ozdelen, G. Tuncman, C. Gorgun, L. H. Glimcher, G. S. Hotamisligil, Endoplasmic reticulum stress links obesity, insulin action, and type 2 diabetes. *Science* **306**, 457–461 (2004).

51. M. K. Brown, N. Naidoo, The endoplasmic reticulum stress response in aging and age-related diseases. *Front. Physiol.* **3**, 263 (2012).

52. L. Qi, B. Tsai, P. Arvan, New insights into the physiological role of endoplasmic reticulum-associated degradation. *Trends Cell Biol.* **27**, 430–440 (2017).

53. R. Covino, S. Ballweg, C. Stordeur, J. B. Michaelis, K. Puth, F. Wernig, A. Bahrami, A. M. Ernst, G. Hummer, R. Ernst, A eukaryotic sensor for membrane lipid saturation. *Mol. Cell* **63**, 49–59 (2016).

54. K. Halbleib, K. Pesek, R. Covino, H. F. Hofbauer, D. Wunnicke, I. Hanelt, G. Hummer, R. Ernst, Activation of the unfolded protein response by lipid bilayer stress. *Mol. Cell* **67**, 673–684.e8 (2017).

55. Y. Chang, A. Abe, J. A. Shayman, Ceramide formation during heat shock: A potential mediator of alpha B-crystallin transcription. *Proc. Natl. Acad. Sci. U.S.A.* **92**, 12275–12279 (1995).

56. R. C. Dickson, E. E. Nagiec, M. Skrzypek, P. Tillman, G. B. Wells, R. L. Lester, Sphingolipids are potential heat stress signals in Saccharomyces. *J. Biol. Chem.* **272**, 30196–30200 (1997).

57. G. M. Jenkins, A. Richards, T. Wahl, C. Mao, L. Obeid, Y. Hannun, Involvement of yeast sphingolipids in the heat stress response of Saccharomyces cerevisiae. *J. Biol. Chem.* **272**, 32566–32572 (1997).

58. Y. Niimura, T. Moue, N. Takahashi, K. Nagai, Modification of sphingoglycolipids and sulfolipids in kidney cell lines under heat stress: Activation of monohexosylceramide synthesis as a ceramide scavenger. *Glycobiology* **20**, 710–717 (2010).

59. G. B. Wells, R. C. Dickson, R. L. Lester, Heat-induced elevation of ceramide in Saccharomyces cerevisiae via de novo synthesis. *J. Biol. Chem.* **273**, 7235–7243 (1998).

60. S. M. Turpin-Nolan, J. C. Bruning, The role of ceramides in metabolic disorders: When size and localization matters. *Nat. Rev. Endocrinol.* **16**, 224–233 (2020).

61. S. Borodzicz, K. Czarzasta, M. Kuch, A. Cudnoch-Jedrzejewska, Sphingolipids in cardiovascular diseases and metabolic disorders. *Lipids Health Dis.* **14**, 55 (2015).

62. R. S. Seelan, C. Qian, A. Yokomizo, D. G. Bostwick, D. I. Smith, W. Liu, Human acid ceramidase is overexpressed but not mutated in prostate cancer. *Genes Chromosomes Cancer* **29**, 137–146 (2000).

63. C. Cozma, M. I. Iurascu, S. Eichler, M. Hovakimyan, O. Brandau, S. Zielke, T. Bottcher, A. K. Giese, J. Lukas, A. Rolfs, C26-ceramide as highly sensitive biomarker for the diagnosis of Farber disease. *Sci. Rep.* **7**, 6149 (2017).

64. T. Harayama, H. Riezman, Understanding the diversity of membrane lipid composition. *Nat. Rev. Mol. Cell Biol.* **19**, 281–296 (2018).

65. J. Stevenson, E. Y. Huang, J. A. Olzmann, Endoplasmic reticulum-associated degradation and lipid homeostasis. *Annu. Rev. Nutr.* **36**, 511–542 (2016).

66. M. Megyeri, H. Riezman, M. Schuldiner, A. H. Futerman, Making sense of the yeast sphingolipid pathway. *J. Mol. Biol.* **428**, 4765–4775 (2016).

67. A. Finger, M. Knop, D. H. Wolf, Analysis of two mutated vacuolar proteins reveals a degradation pathway in the endoplasmic reticulum or a related compartment of yeast. *Eur. J. Biochem.* **218**, 565–574 (1993).

68. E. D. Spear, D. T. Ng, Stress tolerance of misfolded carboxypeptidase Y requires maintenance of protein trafficking and degradative pathways. *Mol. Biol. Cell* **14**, 2756–2767 (2003).

69. V. Cerantola, I. Guillas, C. Roubaty, C. Vionnet, D. Uldry, J. Knudsen, A. Conzelmann, Aureobasidin A arrests growth of yeast cells through both ceramide intoxication and deprivation of essential inositolphosphorylceramides. *Mol. Microbiol.* **71**, 1523–1537 (2009).

70. K. Nakatsukasa, T. Nishimura, S. D. Byrne, M. Okamoto, A. Takahashi-Nakaguchi, H. Chibana, F. Okumura, T. Kamura, The ubiquitin ligase SCF(Ucc1) acts as a metabolic switch for the glyoxylate cycle. *Mol. Cell* **59**, 22–34 (2015).

71. H. Yu, A. K. Singh Gautam, S. R. Wilmington, D. Wylie, K. Martinez-Fonts, G. Kago, M. Warburton, S. Chavali, T. Inobe, I. J. Finkelstein, M. M. Babu, A. Matouschek, Conserved sequence preferences contribute to substrate recognition by the proteasome. *J. Biol. Chem.* **291**, 14526–14539 (2016).

72. T. Hashida-Okado, A. Ogawa, M. Endo, R. Yasumoto, K. Takesako, I. Kato, AUR1, a novel gene conferring aureobasidin resistance on Saccharomyces cerevisiae: A study of defective morphologies in Aur1p-depleted cells. *Mol. Gen. Genet.* **251**, 236–244 (1996).

73. S. A. Heidler, J. A. Radding, The AUR1 gene in Saccharomyces cerevisiae encodes dominant resistance to the antifungal agent aureobasidin A (LY295337). *Antimicrob. Agents Chemother.* **39**, 2765–2769 (1995).

74. X. H. Fun, G. Thibault, Lipid bilayer stress and proteotoxic stress-induced unfolded protein response deploy divergent transcriptional and non-transcriptional programmes. *Biochim. Biophys. Acta Mol. Cell Biol. Lipids* **1865**, 158449 (2020).

75. P. I. Merksamer, A. Trusina, F. R. Papa, Real-time redox measurements during endoplasmic reticulum stress reveal interlinked protein folding functions. *Cell* **135**, 933–947 (2008).

76. K. Sato, Y. Noda, K. Yoda, Kei1: A novel subunit of inositolphosphorylceramide synthase, essential for its enzyme activity and Golgi localization. *Mol. Biol. Cell* **20**, 4444–4457 (2009).

77. I. Guillas, P. A. Kirchman, R. Chuard, M. Pfefferli, J. C. Jiang, S. M. Jazwinski, A. Conzelmann, C26-CoA-dependent ceramide synthesis of Saccharomyces cerevisiae is operated by Lag1p and Lac1p. *EMBO J.* **20**, 2655–2665 (2001).

78. W. I. Wu, V. M. McDonough, J. T. Nickels Jr., J. Ko, A. S. Fischl, T. R. Vales, A. H. Merrill Jr., G. M. Carman, Regulation of lipid biosynthesis in Saccharomyces cerevisiae by fumonisin B1. *J. Biol. Chem.* **270**, 13171–13178 (1995).

79. S. Epstein, G. A. Castillon, Y. Qin, H. Riezman, An essential function of sphingolipids in yeast cell division. *Mol. Microbiol.* **84**, 1018–1032 (2012).

80. C. S. Ejsing, J. L. Sampaio, V. Surendranath, E. Duchoslav, K. Ekroos, R. W. Klemm, K. Simons, A. Shevchenko, Global analysis of the yeast lipidome by quantitative shotgun mass spectrometry. *Proc. Natl. Acad. Sci. U.S.A.* **106**, 2136–2141 (2009).

81. C. S. Oh, D. A. Toke, S. Mandala, C. E. Martin, ELO2 and ELO3, homologues of the Saccharomyces cerevisiae ELO1 gene, function in fatty acid elongation and are required for sphingolipid formation. *J. Biol. Chem.* **272**, 17376–17384 (1997).

82. S. Dasgupta, J. Kong, E. Bieberich, Phytoceramide in vertebrate tissues: One step chromatography separation for molecular characterization of ceramide species. *PLOS ONE* **8**, e80841 (2013).

83. F. Omae, M. Miyazaki, A. Enomoto, M. Suzuki, Y. Suzuki, A. Suzuki, DES2 protein is responsible for phytoceramide biosynthesis in the mouse small intestine. *Biochem. J.* **379**, 687–695 (2004).

84. B. Chaurasia, S. A. Summers, Ceramides in metabolism: Key lipotoxic players. *Annu. Rev. Physiol.* **83**, 303–330 (2021).

85. Y. A. Hannun, L. M. Obeid, Principles of bioactive lipid signalling: Lessons from sphingolipids. *Nat. Rev. Mol. Cell Biol.* **9**, 139–150 (2008).

86. A. P. Seitz, H. Grassme, M. J. Edwards, Y. Pewzner-Jung, E. Gulbins, Ceramide and sphingosine in pulmonary infections. *Biol. Chem.* **396**, 611–620 (2015).

87. N. Beckmann, K. A. Becker, Ceramide and related molecules in viral infections. *Int. J. Mol. Sci.* **22**, 5676 (2021).

88. D. C. Barbacci, A. Roux, L. Muller, S. N. Jackson, J. Post, K. Baldwin, B. Hoffer, C. D. Balaban, J. A. Schultz, S. Gouty, B. M. Cox, A. S. Woods, Mass spectrometric imaging of ceramide biomarkers tracks therapeutic response in traumatic brain injury. *ACS Chem. Nerosci.* **8**, 2266–2274 (2017).

89. G. Wang, E. Bieberich, Sphingolipids in neurodegeneration (with focus on ceramide and S1P). *Adv. Biol. Regul.* **70**, 51–64 (2018).

90. Y. Jo, P. C. Lee, P. V. Sguigna, R. A. DeBose-Boyd, Sterol-induced degradation of HMG CoA reductase depends on interplay of two Insigs and two ubiquitin ligases, gp78 and Trc8. *Proc. Natl. Acad. Sci. U.S.A.* **108**, 20503–20508 (2011).

91. S. Gulati, Y. Liu, A. B. Munkacsi, L. Wilcox, S. L. Sturley, Sterols and sphingolipids: Dynamic duo or partners in crime? *Prog. Lipid Res.* **49**, 353–365 (2010).

92. E. Swain, K. Baudry, J. Stukey, V. McDonough, M. Germann, J. T. Nickels Jr., Sterol-dependent regulation of sphingolipid metabolism in Saccharomyces cerevisiae. *J. Biol. Chem.* **277**, 26177–26184 (2002).

93. A. B. Garcia-Arribas, A. Alonso, F. M. Goni, Cholesterol interactions with ceramide and sphingomyelin. *Chem. Phys. Lipids* **199**, 26–34 (2016).

94. B. Chaurasia, T. S. Tippetts, R. Mayoral Monibas, J. Liu, Y. Li, L. Wang, J. L. Wilkerson, C. R. Sweeney, R. F. Pereira, D. H. Sumida, J. A. Maschek, J. E. Cox, V. Kaddai, G. I. Lancaster, M. M. Siddique, A. Poss, M. Pearson, S. Satapati, H. Zhou, D. G. McLaren, S. F. Previs, Y. Chen, Y. Qian, A. Petrov, M. Wu, X. Shen, J. Yao, C. N. Nunes, A. D. Howard, L. Wang, M. D. Erion, J. Rutter, W. L. Holland, D. E. Kelley, S. A. Summers, Targeting a ceramide double bond improves insulin resistance and hepatic steatosis. *Science* **365**, 386–392 (2019).

95. M. To, C. W. Peterson, M. A. Roberts, J. L. Counihan, T. T. Wu, M. S. Forster, D. K. Nomura, J. A. Olzmann, Lipid disequilibrium disrupts ER proteostasis by impairing ERAD substrate glycan trimming and dislocation. *Mol. Biol. Cell* **28**, 270–284 (2017).

96. L. K. Liu, V. Choudhary, A. Toulmay, W. A. Prinz, An inducible ER-Golgi tether facilitates ceramide transport to alleviate lipotoxicity. *J. Cell Biol.* **216**, 131–147 (2017).

97. H. Sawai, Y. Okamoto, C. Luberto, C. Mao, A. Bielawska, N. Domae, Y. A. Hannun, Identification of ISC1 (YER019w) as inositol phosphosphingolipid phospholipase C in Saccharomyces cerevisiae. *J. Biol. Chem.* **275**, 39793–39798 (2000).

98. G. van Meer, D. R. Voelker, G. W. Feigenson, Membrane lipids: Where they are and how they behave. *Nat. Rev. Mol. Cell Biol.* **9**, 112–124 (2008).

99. L. Silva, R. F. de Almeida, A. Fedorov, A. P. Matos, M. Prieto, Ceramide-platform formation and -induced biophysical changes in a fluid phospholipid membrane. *Mol. Membr. Biol.* **23**, 137–148 (2006).

100. J. T. Marques, A. M. Cordeiro, A. S. Viana, A. Herrmann, H. S. Marinho, R. F. de Almeida, Formation and properties of membrane-ordered domains by phytoceramide: Role of sphingoid base hydroxylation. *Langmuir* **31**, 9410–9421 (2015).

101. R. Prasad, A. Sliwa-Gonzalez, Y. Barral, Mapping bilayer thickness in the ER membrane. *Sci. Adv.* **6**, eaba5130 (2020).

102. R. S. Sikorski, P. Hieter, A system of shuttle vectors and yeast host strains designed for efficient manipulation of DNA in Saccharomyces cerevisiae. *Genetics* **122**, 19–27 (1989).

103. R. D. Gietz, R. H. Schiestl, High-efficiency yeast transformation using the LiAc/SS carrier DNA/PEG method. *Nat. Protoc.* **2**, 31–34 (2007).

104. R. Gardner, S. Cronin, B. Leader, J. Rine, R. Hampton, Sequence determinants for regulated degradation of yeast 3-hydroxy-3-methylglutaryl-CoA reductase, an integral endoplasmic reticulum membrane protein. *Mol. Biol. Cell* **9**, 2611–2626 (1998).

105. C. Klose, M. A. Surma, M. J. Gerl, F. Meyenhofer, A. Shevchenko, K. Simons, Flexibility of a eukaryotic lipidome—Insights from yeast lipidomics. *PLOS ONE* **7**, e35063 (2012).

106. M. A. Surma, R. Herzog, A. Vasilj, C. Klose, N. Christinat, D. Morin-Rivron, K. Simons, M. Masoodi, J. L. Sampaio, An automated shotgun lipidomics platform for high throughput, comprehensive, and quantitative analysis of blood plasma intact lipids. *Eur. J. Lipid Sci. Technol.* **117**, 1540–1549 (2015).

107. G. Liebisch, M. Binder, R. Schifferer, T. Langmann, B. Schulz, G. Schmitz, High throughput quantification of cholesterol and cholesteryl ester by electrospray ionization tandem mass spectrometry (ESI-MS/MS). *Biochim. Biophys. Acta* **1761**, 121–128 (2006).

108. R. Herzog, D. Schwudke, K. Schuhmann, J. L. Sampaio, S. R. Bornstein, M. Schroeder, A. Shevchenko, A novel informatics concept for high-throughput shotgun lipidomics based on the molecular fragmentation query language. *Genome Biol.* **12**, R8 (2011).

109. R. Herzog, K. Schuhmann, D. Schwudke, J. L. Sampaio, S. R. Bornstein, M. Schroeder, A. Shevchenko, LipidXplorer: A software for consensual cross-platform lipidomics. *PLOS ONE* **7**, e29851 (2012).